POPULUS FREMONTII TREE RING ANALYSIS AND SEMI-ARID RIVER WATER SOURCE VARIABILITY OVER TIME, SAN PEDRO RIVER, ARIZONA

by

Rebecca Stolar

A Thesis Submitted to the Faculty of the

DEPARTMENT OF HYDROLOGY & ATMOSPHERIC SCIENCES

In Partial Fulfillment of the Requirements

For the Degree of

MASTER OF SCIENCE

WITH A MAJOR IN HYDROLOGY

In the Graduate College

THE UNIVERSITY OF ARIZONA

2019

THE UNIVERSITY OF ARIZONA
GRADUATE COLLEGE

As members of the Master's Committee, we certify that we have read the thesis prepared by Rebecca Stolar, titled *Populus fremontii tree ring analysis and semi-arid river water source variability over time, San Pedro River, Arizona* and recommend that it be accepted as fulfilling the dissertation requirement for the Master's Degree.

Thomas Meixner Date: 4/23/19

Jia Hu Date: 4/23/19

Guo-Yue Niu Date: 4/23/2019

Final approval and acceptance of this thesis is contingent upon the candidate's submission of the final copies of the thesis to the Graduate College.

I hereby certify that I have read this thesis prepared under my direction and recommend that it be accepted as fulfilling the Master's requirement.

Thomas Meixner Date: 5/20/19
Master's Thesis Committee Chair
Hydrology and Atmospheric Sciences Department

ACKNOWLEDGEMENTS

Thank you to Dr. Christopher Sargeant and Dr. Michael Singer for their extensive help with the inversion of the Barbour model. To Dr. Russ Scott for providing and aiding in manipulation of hydrometeorological data. To Dr. Jia Hu for your patience, understanding, and extensive knowledge on tree mechanisms and to Dr. Thomas Meixner for your continuous encouragement on this project. Special thank you to my family and Jack for the love and support.

TABLE OF CONTENTS

Page

LIST OF TABLES

LIST OF FIGURES

NOMECLATURE

Transpiration rate	ET
Relative Humidity	RH
Stomatal conductance	g_s
Boundary layer conductance	g_b
Effective path length	L
Temperature of air	T_a
Leaf temperature	T_L
Leaf temperature difference	T_{diff}
Concentration of water	$[H_2O]$
Saturated vapor pressure of air	e_{sat}
Actual vapor pressure of air	e_{air}
Leaf internal vapor pressure	e_{leaf}
$\Delta^{18}O$ of water vapor	$\Delta^{18}O_{wv}$
Equilibrium fractionation between C=O and water	ε_{wc}
Equilibrium vapor pressure fractionation	ε_e
Total diffusive fractionation	ε_{diff}
Diffusive fractionation through stomata	ε_{ks}
Diffusive fractionation through boundary layer	ε_{kb}
Diffusivity of $H_2{}^{18}O$ in water	D
Craig-Gordon Evaporation-site water	δ_e
Bulk Leaf Water	$\Delta^{18}O_L$, $\delta^{18}O_L$
Peclet number	$\wp$
Proportion of xylem water in meristem	p_x
Proportion of exchangeable oxygen in cellulose	p_{ex}
$^{18}O/^{16}O$ of water vapor	δ_{wv}
$^{18}O/^{16}O$ of source water	δ_{sw}
$^{18}O/^{16}O$ SMOW	δ_{SMOW}
$\Delta^{18}O$ Sucrose	$\Delta^{18}O_{suc}$
$\Delta^{18}O$ Cellulose	$\Delta^{18}O_{cell}$
$\delta^{18}O$ predicted cellulose	$\delta^{18}O_{pcell}$
$\delta^{18}O$ measured cellulose	$\delta^{18}O_{cell}$
$\delta^{18}O$ atmospheric water vapor	$\delta^{18}O_{wv}$
$\delta^{18}O$ modelled source water	$\delta^{18}O_{mod}$
$\delta^{18}O$ stream water	$\delta^{18}O_{sw}$

ABSTRACT

Stolar, Rebecca. M.S. Hydrology, University of Arizona, May 2019. *Populus fremontii* tree ring analysis and semi-arid river water source variability over time, San Pedro River, Arizona Major Professor: Thomas Meixner.

Summer floods are an important source of sustained streamflow in arid and semi-arid rivers of the American Southwest and Northwest Mexico. The degree to which natural function versus human alterations influence the system is subject to debate. Environmental information in the tree ring cellulose of *Populus* can be used to investigate the variation in water sources over time in these areas. Past research has shown that streamflow sources in the San Pedro Basin of Arizona vary isotopically between a source water of basin ground water and a summer flood water source. This study uses isotopic analyses of *Populus fremontii* and atmospheric data in the San Pedro Basin to estimate the water source of the trees and the river water source condition. After analyzing weather data within the basin, an inversion of the Barbour oxygen isotope model using tree ring cellulose isotopes was used to obtain the water source isotopic composition. The variation in water source composition inferred from the model was then compared to the river composition over time. It was initially found that each site's water source isotopic composition was significantly different from the source water. However, several water source isotopic compositions were found to be more negative than the known basin groundwater signature in each of the study sites. Following sensitivity analyses on various parameters within the model, it was seen that relative humidity has a strong influence on the determination of source water. Therefore, relative humidity must be an accurate measurement and is not considered to be so in this study. Furthermore, in order to understand the degree to which natural function versus human alterations influence the system, older *Populus fremontii* tree ring isotopes are needed, posing a question regarding the reliability of the species.

Chapter 1: INTRODUCTION

Riparian ecosystems in the western US experience dramatic interannual fluctuations in water availability in comparison to the surrounding desert environment. Summer floods greatly influence the growing season throughout the year. Due to highly variable precipitation and streamflow, there are also variations in growing conditions each year. In *Populus fremontii* (*P. fremontii),* this variation among years can be seen through tree ring carbon isotope composition ($\delta^{13}C$), influenced by streamflow, local precipitation, and temperature. In a study completed by Leffler and Evans (1990), streamflow was seen to be the primary climactic factor influencing *P. fremontii* with tree growth occurring in the months of May and June, impacting the $\delta^{13}C$ of tree ring tissue. In years of low streamflow, the intense monsoons, accounting for >50% of the total annual precipitation for some years, provided the needed water during the growing season (Leffler and Evans, 1999).

P. fremontii is an important riparian vegetation species in the American Southwest and has been studied at the whole tree and leaf levels with a focus on riparian restoration due to *Tamarix* invasions (Farid et al., 2007; Schaefer et al., 2000; Gazal et al., 2006; Kochendorfer et al., 2010). Farid et al. (2007) used airborne lidar to provide LAI estimates to improve corridor-level riparian water-use estimates. This allows for large areas to be analyzed. Using sap flow, Gazal et al. (2006) found that seasonal fluctuations of transpiration in *P. fremontii* closely follow water table variations along intermittent reaches of the San Pedro River. As groundwater depths increase during stress periods, *P. fremontii* shows reduced CO_2 uptake and ET (Kochendorfer et al., 2010). Therefore, with the changes

in groundwater depth, these stress periods greatly influence the growing season and alter growing conditions each year.

The summer flood water provides stream flow that *P. fremontii* uses as a source water in the San Pedro Basin. Figure 1.1 illustrates the summer stream flow along a section of the San Pedro River described later. This shows that the summer streamflow has seen high variability since 1990, particularly after approximately 2005. This variation aides in explaining natural functions of the river system when compared to the modelled source water of *P. fremontii.*

Oxygen isotope ratios within tree ring cellulose ($\delta^{18}O_{cell}$) aide in further determining the source water of phreatophytes, plants with deep root systems, throughout the year (Roden and Ehleringer, 1999). These isotopic ratios can be used in models to predict the source water, or vice versa and given humidity and source water environmental information, can predict the isotope ratios of tree-rings (Rodel et al., 1999). Barbour et al. (2004) demonstrated successful predictions of $\delta^{18}O_{cell}$ from known source water signatures. By accounting for various environmental and physical variables, Sargeant and Singer (2016) produced an inversion of the Barbour model.

The purpose of this study is to compare the variation in water source composition in *P. fremontii* to river composition over time. How well did the inversion of the Barbour model produced by Sargeant and Singer (2016) initially predict $\delta^{18}O_{mod}$ for each site given the initial set of parameters? Which parameters are the most sensitive and how do they influence the model? How did years of high summer stream flow differ from years of low summer streamflow? What needs to be measured in order to produce more accurate $\delta^{18}O_{mod}$ results? How reliable are *P. fremontii*? To answer these questions, the modelled source

water of the trees was estimated through isotopic analyses of *P. fremontii* cellulose and atmospheric data in the San Pedro Basin and then compared to river water source composition. After interpreting weather data within the basin, an inversion of the Barbour model using tree ring cellulose isotopes collected and analyzed from *P. fremontii* was used to obtain the water source isotopic composition. The variation in water source composition as inferred from the inverse Barbour model was then compared to river composition over time. By drawing this comparison, it aides in anticipating consequences from human driven modification including climate change and groundwater pumping on the river systems.

Chapter 2: STUDY AREA

2.1 Site Description

This study focused on Southeastern Arizona along the Upper San Pedro River, a north flowing river originating in Northern Mexico. Specifically, the three sites are within the San Pedro Riparian National Conservation Area (SPRNCA). SPRNCA was formed in November 1988, designating 40 miles of the Upper San Pedro River as a Riparian National Conservation Area in order to protect and enhance the desert riparian ecosystem. This area is of particular interest due to extensive anthropogenic influence. Water depletion from surrounding towns and overgrazing by livestock have greatly influenced the floodplain, shifting much of the biota to *Tamarix* dominant (Brookshire et al., 2010). *Tamarix* is known to alter hydrologic and ecosystem properties (Vitousek, 1990). The data analyzed were from three study sites located on a 16-km north-south transect from Palominas, north to Lewis Springs and Boquillas (Figure 2.1). The three sites represent a gradient in streamflow and groundwater on an annual basis. The Lewis Springs site is perennial, whereas the

Palominas and Boquillas sites are intermittent, with Boquillas being the driest site (Table 2.1).

2.2 Site Hydroclimatology

Climate data including temperature, relative humidity, and barometric pressure were obtained from the Southwest Watershed Research Center at the U.S. Department of Agriculture, Agriculture Research Service (Southwest Watershed Research Center, 2017). Several flux towers were considered based on study site locations and years of data available including the Charleston Mesquite Woodland, Lewis Springs East (Mesquite), and Lucky Hills (Walnut Gulch) sites (Table 2.2). Each of these sites contained various years of data - the Lucky Hills (Walnut Gulch) site contained the most data from 1990 to 2016. In terms of amount of data, this Lucky Hills (Walnut Gulch) site matched the best with the available measured $\delta^{18}O$ cellulose ($\delta^{18}O_{cell}$) for each study site (Palominas, Lewis Springs, and Boquillas) from 1990 to 2015. In order to determine if the Lewis Springs (Walnut Gulch) site could be used for each of the three study sites site (Palominas, Lewis Springs, and Boquillas), the data from the Charleston Mesquite Woodland and Lewis Springs East (Mesquite) flux towers were compared to the Lewis Springs (Walnut Gulch) site. There was not a large difference seen between the Charleston Mesquite Woodland, Lewis Springs East (Mesquite), and Lucky Hills (Walnut Gulch) sites; therefore, no correction factor was included between sites and the Lucky Hills (Walnut Gulch) data was used for the three study sites (Palominas, Lewis Springs, and Boquillas).

Chapter 3: BACKGROUND ON PERTINENT ISOTOPES

3.1 $\delta^{18}O$

Oxygen isotope ratios within tree ring cellulose ($\delta^{18}O_{cell}$) aide in further determining the source water of phreatophytes, plants with deep root systems, throughout the year (Roden et al, 1999; Roden and Ehleringer, 1999). Understanding the flow of water through the river and tree systems allows for the construction of a more precise source water model (Figure 3.1). The initial signature of water is seen in the $\delta^{18}O$ precipitation. This is then discharged through rain, specifically monsoon summer flooding into the stream. The stream discharge is considered to be in equilibrium with the $\delta^{18}O$ precipitation. The $\delta^{18}O$ stream discharge ($\delta^{18}O_{sw}$) becomes more negative as is moves through the subsurface and becomes regional groundwater (Sargeant and Singer, 2019). These two sources of water, stream water and basin groundwater, are taken up by the phreatophytes and the $\delta^{18}O$ sources of each are stored in the cellulose along with the $\delta^{18}O_{wv}$ signature (Sargeant and Singer, 2019). This is modified by fractionation mechanisms within the phreatophyte at the leaf level from meteorological and physiological processes (Sargeant and Singer, 2016). Barbour et al. (2004) demonstrated successful predictions of $\delta^{18}O_{cell}$ from known source water signatures. By accounting for various environmental and physical variables, Sargeant and Singer (2016) produced an inversion of the Barbour model.

Chapter 4: METHODS

4.1 Field Sampling

4.1.1 Tree Cores

Tree core samples were obtained from Meixner et al. (2016). At each site six trees were cored with two to three core samples per tree. Each sample was cross dated in the Lab of Tree-Ring Research at the University of Arizona and ring boundaries were marked directly on the cores. Excluding 1995, where the rings of each tree were separately processed to cellulose, individual rings from 1990-2015 were separated from two cores per tree with a scalpel and then pooled together for processing to cellulose. Samples were ground to 20-mesh in a Wiley Mill and sealed in digestion pouches. The cellulose wood component was isolated by first dissolving extractives with toluene and ethanol in a Soxhlet, boiling in deionized water, oxidizing lignin with an acidified $NaClO_3$ solution, and dissolving hemicellulose with an NaOH solution. The resulting a-cellulose was analyzed on a Finnigan Delta Plus mass spectrometer in the Environmental Isotope Lab at the University of Arizona for $\delta^{13}C$ and $\delta^{18}O_{cell}$ (Figure 4.1) with respect to the PDB and SMOW standards. (Meixner et al., 2016)

4.1.2 Water Source Identification

Measured $\delta^{18}O$ stream water data ($\delta^{18}O_{sw}$) was obtained from Meixner et al. (2016) at each of the three study locations from approximately 1994 to 2016. The majority of these measurements ranged from the years 1999 to 2015, as seen in Figure 4.2. The $\delta^{18}O_{sw}$ ranged from approximately -6‰ to approximately -8‰. For the purposes of this study, the $\delta^{18}O_{sw}$ was considered to be in equilibrium with monsoon flow and precipitation. The $\delta^{18}O_{sw}$ is

seen to be less negative than the $\delta^{18}O$ basin ground water when plotted on the Local Meteoric Water Line (LMWL) (Baillie et al., 2007; Figure 4.3). Baillie et al. (2007) previously detailed the riparian and baseflow samples in several study areas surrounding the study sites discussed here. A weighted linear regression of all precipitation samples in the Baillie et al. (2007) study yielded the below relationship between $\delta^{2}H$ and $\delta^{18}O$ values (Equation 1). Here the trend line equations for summer and winter flooding are also shown: summer precipitation representing a lower slope than the global meteoric water line potentially indicating evaporation and winter precipitation with a higher slope suggesting less control from evaporation (Baillie et al., 2007).

$$\delta^{2}H = (7.1 \pm 0.4) * \delta^{18}O + (3.1 \pm 3.1) \quad \text{A}$$

$$\delta^{2}H = (6.8 \pm 1.5) * \delta^{18}O + (0.4 \pm 9.4) \quad \text{B}$$

$$\delta^{2}H = (8.6 \pm 0.6) * \delta^{18}O + (20.4 \pm 7.0) \quad \text{C}$$

Equation 1 (Baillie et al., 2007) A) A weighted linear regression of all precipitation samples from Baillie et al. (2007). B) Summer precipitation trend line. C) Winter precipitation trend.

4.2 Modeling Annual Source Water Use

To determine the source water of the trees, an inverse of the Barbour et al. (2004) model produced by Sargeant and Singer (2016) was used. The inverse model was coded in Microsoft Excel (version 2016), predicting the $\delta^{18}O$ source water ($\delta^{18}O_{mod}$) from known $\delta^{18}O_{cell}$ (Singer et al., 2018). While there were many constraints within the model, the following were the only altered parameters from those provided (Singer et al., 2018): mean air temperature (T_a), average annual relative humidity (RH), and atmospheric water vapor ($\delta^{18}O_{wv}$). An average stomatal conductance was obtained from Pataki et al. (2005) at a value of 0.075 mol m^{-2} s^{-1}. An average boundary layer conductance was calculated from

Farid et al. (2008) using the reciprocal of the boundary layer resistance equation (Equation 2). It was found to be approximately 1.78 mol m^{-2} s^{-1}. This equation incorporated the Leaf Area Index (LAI), a scaling factor, an attenuation coefficient for wind speed inside the canopy, a typical leaf width for *P. fremontii*, and the wind speed outside the canopy (Equation 2). Wind speeds were obtained from the Southwest Watershed Research Center at the U.S. Department of Agriculture, Agriculture Research Service (Southwest Watershed Research Center, 2017). Two transpiration rates were used, one for the intermittent sites (Boquillas and Palominas), and one for the perennial site (Lewis Springs). These transpiration rates were obtained from Farid et al. (2008) at values of approximately 1.29 mmol m^{-2} s^{-1} for the intermittent sites and approximately 3.22 mmol m^{-2} s^{-1} for the perennial site.

$$r_b = \frac{1}{(LAI)(b)} \frac{\propto_{att}}{(1 - \exp(-(1/2) \propto_{att}))} \sqrt{\frac{\omega}{U}}$$

Equation 2 Boundary layer resistance equation (Farid et al., 2008). Where LAI is the Leaf Area Index and is 3.48 for the perennial site and 2.78 for the intermittent sites. b is 0.0067 m $s^{-1/2}$ and is a scaling coefficient for leaf boundary layer resistance (Magnani et al., 1998). α_{att} is an attenuation coefficient for wind speed inside the canopy, ω is 0.05 m and is a typical leaf width, and U is the wind speed outside the canopy (obtained from the Southwest Watershed Research Center at the U.S. Department of Agriculture, Agriculture Research Service (Southwest Watershed Research Center, 2017).

To characterize the $\delta^{18}O_{wv}$ needed for the inverse model, it was assumed that precipitation and atmospheric water vapor were in isotopic equilibrium. The $\delta^{18}O_{wv}$ was approximated from Bowen (2019) as seen in Figure 4.4. Assuming atmospheric water vapor being one of the three main contributing constraints (air temperature and relative humidity being the other two), a low, average, and high value were initially used for the given range. An offset of 10‰ from the precipitation measurement was applied to account

for the mixing region and dynamic effects of air mass origin (Sargeant and Singer, 2016; Bowen and Wilkinson, 2002; Celle-Jeanton et al., 2001; Delattre et al., 2015).

After producing the initial $\delta^{18}O_{mod}$ results, discussed later, ANOVA tests reported to the 95% significance level showed that the low, average, and high values were not significantly different at each site. P values for these ANOVA tests at the Palominas, Lewis Springs, and Boquillas sites were found to be 0.078, 0.240, and 0.067, respectively. Due to this significant similarity, the average $\delta^{18}O_{wv}$ was used for the remainder of the study.

The inversion of the Barbour et al. (2004) model produced by Sargeant and Singer (2016) used included various hydrologic and tree mechanistic equations in order to predict the $\delta^{18}O_{mod}$ from known $\delta^{18}O_{cell}$. The following are constants and select, influential equations included in the model (Table 4.3; Equations 3-9).

$$L = (0.0000236) * (ET)^{1.2}$$

Equation 3 Effective path length (Song et al., 2013) where L is a single power function and ET is the leaf transpiration rate.

$$\wp = \frac{ET * L}{[H_2O] * D}$$

Equation 4 Péclet number (Barbour et al., 2004) where L is the effective path length, ET is the transpiration rate, $[H_2O]$ is the molar density of water and D is the diffusivity of the $H_2{}^{18}O$ in water.

$$\Delta^{18}O_{cell} = (\Delta^{18}O_L * [1 - (p_x * p_{ex})]) + \varepsilon_{wc}$$

Equation 5 Cellulose $\Delta^{18}O$ (Barbour and Farquhar, 2000) where $\Delta^{18}O_L$ is the bulk leaf water, p_x and p_{ex} are the proportion of xylem water in meristem and the proportion of exchangeable oxygen in cellulose, respectively, and ε_{wc} is the equilibrium fractionation between C=O and water.

$$\delta_e = \delta_{sw} + \varepsilon_{ks} + \varepsilon_{kb} + D + [\delta_{wv} - \delta_{sw} - (\varepsilon_{ks} + \varepsilon_{kb})] * \frac{e_{air}}{e_{leaf}}$$

Equation 6 Craig-Gordon Evaporation-site water (Barbour et al., 2004) where δ_e, δ_{Sw}, and δ_{wv} are the oxygen isotopic compositions of water at the evaporating sites, source water, and atmospheric water vapor, respectively.

ε_{ks}+ ε_{kb} is the kinetic fractionation as water vapor diffuses through the stomata and the boundary layer. D is the fractionation associated with the proportional depression of water vapor by $H_2{}^{18}O$.

$$\Delta^{18}O_L = \frac{\delta_e * [1 - EXP(\wp)]}{\wp}$$

Equation 7 Bulk Leaf Water (Farquhar and Lloyd, 1993) where δ_e is the oxygen isotopic compositions of water at the evaporating sites and $\wp$ is the Péclet effect.

$$\varepsilon_{diff} = \frac{\frac{1}{g_s} * \varepsilon_{ks} + \left(\frac{1}{g_b} * \varepsilon_{kb}\right)}{\frac{1}{g_b} + \frac{1}{g_s}}$$

Equation 8 Total diffusive fractionation (Farquhar et al., 1989) where g_s and g_b are the stomatal conductance and boundary layer conductance, respectively. ε_{ks} and ε_{kb} are the diffusive fractionations through the and boundary layer, respectively.

$$\varepsilon_e = 1000 * \left(EXP\left[\frac{1137}{(T_L + 273.16)^2} - \frac{0.4156}{(T_L + 273.16)} - 0.0020667\right] - 1\right)$$

Equation 9 Equilibrium vapor pressure fractionation (Majoube, 1971) where ε_e is the equilibrium vapor pressure fractionation and T_L is the leaf temperature.

4.3 Initial Sensitivity Analyses

Sensitivity analyses were initially completed using root mean squared errors (RMSE) for RH, T_a, and $\delta^{18}O_{wv}$. The RMSE allowed for the representation of how increases in a given parameter fit the initial modelled results. If a given parameter produced small RSME values in comparison to other parameters, it was said to be less sensitive within the model. If a given parameter produced RMSE values less than one, it was not considered to be sensitive.

Initially, RH, T_a, and $\delta^{18}O_{wv}$ were assumed to be the most influential in determining the $\delta^{18}O_{mod}$. Using Excel (version 2016), random numbers were generated between 0 and 1 in order to produce percent increases for each parameter. The same percent increase was

used for RH, T_a, and $\delta^{18}O_{wv}$ for each year, at each site. 20 runs were completed in this manner, producing increases from approximately 5% to 85%. The root mean square error (RMSE) was calculated for each of the 20 runs at each site. Stomatal conductance, boundary layer conductance, and transpiration rates were initially not assumed to be as influential in determining the $\delta^{18}O_{mod}$. This is because these parameters did not vary by year in the model as RH, T_a, and $\delta^{18}O_{wv}$ did suggesting that they were less influential in the equations used within the model.

4.4 Adjusted RH Values

After obtaining the initial $\delta^{18}O_{mod}$ results and the initial sensitivity analysis for RH, T_a, and $\delta^{18}O_{wv}$, it was determined that the RH was the most sensitive to the equations in the model. The initial RH was an average annual value for each year at each site. However, the growing season of *P. fremontii* is approximately March 15 through October 31 and RH varies greatly between day and night. Due to this, the RH was averaged across the adjusted period of the *P. fremontii* growing season during only daylight hours. This altered RH was used to predict a new set of $\delta^{18}O_{mod}$ results and was used for further sensitivity analyses.

4.5 Further Sensitivity Analyses

As previously mentioned, there were several parameters that were not altered from Sargeant and Singer (2016) (Table 4.3). Two of these parameters included the proportion of exchangeable oxygen in cellulose (p_{ex}) and the proportion of xylem water in meristem (p_x). While these parameters are separated as constants in the model (Table 4.3), they are treated as a combined factor in Equation 5 Cellulose $\Delta^{18}O$ (Barbour and Farquhar, 2000).

Following the initial results and the adjusted RH, a small sensitivity analysis was completed for the combined factor $p_{ex}p_x$. The individual parameters p_{ex} and p_x were removed from the model and replaced with the combined $p_{ex}p_x$ term with a range of 0.3 to 0.4 (Barbour et al., 2004).

Following the results of the $p_{ex}p_x$ factor, the effective path length (L) was considered (Equation 3). L was determined to be an influential parameter in the Péclet effect ($\wp$; Equation 4) (Barbour et al., 2004; Barbour and Farquhar, 2000) and to be heavily dependent on leaf transpiration rate (ET) (Song et al., 2013). Song et al. (2013) studied six tree species and found L to equal Equation 3. This single power function fit the data well and showed the relationship of ET (Figure 4.5). However, L is also closely related to p_x and p_{ex} (Barbour et al., 2004). When the equilibrium fractionation between carbonyl oxygen and water (ε_{wc}) is assumed to be 27‰, as in this study (Table 4.3), Barbour et al. (2004) found $p_{ex}p_x$ was 0.3 or 0.4 with L either 0.01 or 0.03 m. For cottonwood trees, the best fit of measured on modelled data was produced when $p_{ex}p_x$=0.4 and L=0.02 m (Barbour et al., 2004; Figure 4.6). For this study, following the combined $p_{ex}p_x$ sensitivity analysis, the model was altered from Sargeant and Singer (2016) and a combined $p_{ex}p_x$ of 0.02 m was used with L=0.4.

4.6 Statistical Analyses

All statistical analyses were conducted in Microsoft Excel (version 2016) and are reported to the 95% significance level. For correlation analyses, the T-test (T) for comparing the means of two sample sets was used, and ANOVA (F) was used for comparing the means of more than two datasets.

Chapter 5: RESULTS AND INTERPRETATIONS

5.1 Potential $\delta^{18}O$ Source Water Signatures

As previously discussed, the $\delta^{18}O_{sw}$ at the three study sites ranged from approximately -6‰ to approximately -8‰ (Figure 4.2). From Baillie et al. (2007), the $\delta^{18}O_{sw}$ was seen to be less negative than the $\delta^{18}O$ basin ground water (Figure 4.3). Based on the $\delta^{18}O_{sw}$ data obtained from Meixner et al. (2016), the stream composition from each of the study sites was compared against each other. Based on the ANOVA test comparing each site $\delta^{18}O_{sw}$, the stream water locations were significantly different from each other ($F=51.11$, $p<0.001$). The average $\delta^{18}O_{sw}$ value for Palominas was -6.66 ± 0.08, Lewis Springs was -7.59 ± 0.04, and Boquillas was -7.20 ± 0.08.

5.2 Initial $\delta^{18}O_{mod}$

Initial $\delta^{18}O_{mod}$ results showed the $\delta^{18}O_{sw}$ and the $\delta^{18}O$ basin groundwater to be significantly less negative than the $\delta^{18}O_{mod}$ across all three study sites (Figures 5.1 through 5.4). The most negative known source water at the sites is the basin groundwater; therefore, the initial $\delta^{18}O_{mod}$ results suggest that the model is not parameterized correctly, discussed later. The Boquillas site predicted $\delta^{18}O_{mod}$ to be the least significantly different from $\delta^{18}O_{sw}$ with a T-test producing a P value of 0.009 as opposed to P values of $6.44x10^{-8}$ and $7.71x10^{-5}$ for the Palominas and Lewis Springs sites, respectively. While there was not annual data available for $\delta^{18}O$ basin groundwater to statistically correlate the $\delta^{18}O_{mod}$ to, figures 3.3 and 3.4 show the $\delta^{18}O_{mod}$ against the LMWL produced by Baillie et al. (2007), previously discussed. This contained an estimate of $\delta^{18}O$ basin groundwater and it was seen that the

$\delta^{18}O_{mod}$ plots well below this value at each of the three study sites. Table 5.1 shows the average $\delta^{18}O_{mod}$ compared to average $\delta^{18}O_{sw}$ and the differences for each site. Boquillas was seen to have the least difference between average $\delta^{18}O_{mod}$ and average $\delta^{18}O_{sw}$ while Palominas was seen to have the greatest difference.

5.3 Initial Sensitivity Analyses for $\delta^{18}O_{mod}$

Sensitivity analyses were completed for RH, T_a, and $\delta^{18}O_{wv}$ as previously described (Figures 5.5 through 5.7). The RMSE for each was calculated with the original $\delta^{18}O_{mod}$ and the randomly generated increased increments from approximately 5% to 85% $\delta^{18}O_{mod}$. Figure 5.5 compared the three parameters, RH, T_a, and $\delta^{18}O_{wv}$ with each site having its own plot. RH was seen to have the highest RMSE of the three parameters at each of the sites thus illustrating that this was the most sensitive parameter in the model. T_a had the lowest RMSE and thus was the least sensitive in the model among the three parameters. The RMSE was found to be less than one for T_a; therefore, T_a was considered not to be a sensitive parameter. These results illustrate that RH was slightly sensitive between the sites whereas T_a and $\delta^{18}O_{wv}$ were not (Figure 5.6).

Focusing on the increases in each parameter, high increases in each value were not realistic for the study sites. These results show that at very low percent increases, water vapor was slightly more sensitive than relative humidity; however, relative humidity became an exponentially more sensitive parameter with higher percent increases (Figure 5.7).

5.4 $\delta^{18}O_{mod}$ with Adjusted RH Values

Following the initial $\delta^{18}O_{mod}$ results, several parameters were reconsidered including RH, p_{ex}, p_x, and L. Beginning with RH, the initial $\delta^{18}O_{mod}$ results were based on an average annual RH value. As previously stated, due to the growing season and high fluctuations in RH between day and night, a new range of RH values was determined. This new set of RH values used only daylight hours during the growing season of March 15 through October 15 of each year. These data resulted in lower values overall versus the initial set with average RH values of 30.12 and 39.45, respectively. RH and $\delta^{18}O_{mod}$ were seen to be positively correlated: as RH decreased, $\delta^{18}O_{mod}$ results were more negative. Therefore, with a new overall lower set of RH values, $\delta^{18}O_{mod}$ were more negative (Figures 5.8 and 5.9). Similar to the initial $\delta^{18}O_{mod}$ results, this did not correlate to the source waters at each of the study sites. This result showed that while RH is a sensitive parameter, it is not the only incorrect parameter in the model.

5.5 Further Sensitivity Analyses

The two parameters, p_{ex} and p_x initially set as constant separate values by Sargeant and Singer (2016) and used as a combined factor in Equation 5 (Barbour and Farquhar, 2000) were subjected to a small sensitivity test. As previously described, the combined factor, $p_{ex}p_x$, replaced the two individual parameters and ranged from 03 to 0.4 (Barbour et al., 2004). Figures 5.10 through 5.13 show the ends of this range demonstrating that a higher $p_{ex}p_x$ resulted in less negative $\delta^{18}O_{mod}$ results. While this parameterization helped, the $\delta^{18}O_{mod}$ were still much lower than the $\delta^{18}O$ groundwater values, the most negative values in the area, thus suggesting more parameterization was needed.

To further enforce this, a high $p_{ex}p_x$ (0.4) was combined with an average L (0.02 m) to result in a set of $\delta^{18}O_{mod}$ which appeared to fit the source water ranges the best (Figures 5.14 and 5.15). As previously mentioned, Barbour et al. (2004) found this $p_{ex}p_x$=0.4 combined with L=0.02 m to best fit cottonwood trees. While there are still outliers in this set, resulting in more negative and some positive $\delta^{18}O_{mod}$, this is likely due to the highest and lowest years of summer flooding at the study site, discussed in more detail later.

Chapter 6: DISCUSSION

6.1 Overview

The three study sites were initially seen to significantly vary in source water, increasing in reliance on stream water as the sites move downstream. There is annual variation throughout the sites, particularly in the years following 2005. This relates to the summer streamflow variability (Figure 1.1) where streamflow appears to become more variable following 2005. However, after several sensitivity analyses on parameters within the model, it was seen that RH greatly influenced $\delta^{18}O_{mod}$ results. While RH available for this study represents the study areas as a whole, the RH at each site appears to vary enough that one set of data cannot be used for all three sites. Furthermore, to fully understand the natural functions versus anthropogenic influences on the river system, earlier $\delta^{18}O_{cell}$ data is needed from older tree rings. However, given the results of this study and that *Populus* trees experience heart rot wood decay (Hickman et al., n.d.), *Populus fremontii* reliability is questioned.

6.2 Initial $\delta^{18}O_{mod}$ given Initial Parameters

As previously stated, the initial $\delta^{18}O_{mod}$ results showed more negative values than the known $\delta^{18}O_{sw}$ and $\delta^{18}O$ basin groundwater for each study site. The $\delta^{18}O$ basin groundwater is the most negative source water available for *P. fremontii*; therefore, there cannot be more negative $\delta^{18}O_{mod}$ than the basin groundwater. This suggests that there were potentially problems with parameters in the model. These could have included constants that should have been equations or vice-versa, constants set at incorrect values, or parameters that were incorrectly calculated. Following these results, the parameters RH, p_{ex}, p_x, and L were focused on.

These initial data results aided in better understanding the model and determining which equations influenced the $\delta^{18}O_{mod}$ results the most. While the initial parameters set by Sargeant and Singer (2016) may have accurately predicted $\delta^{18}O_{mod}$ for a more humid climate such as that along the Rhône River in France, a drier climate such as the San Pedro River would likely need to have a model adapted from the original version.

6.3 Parameter Sensitivity and Model Influence

Parameter sensitivity has shown to aide in narrowing the focus for which equations are most influential in accurately predicting the $\delta^{18}O_{mod}$. The San Pedro River is a drier climate than the Rhône River in France which was used to calibrate the initial model (Sargeant and Singer, 2016). While many of the equations and parameters were consistent between the two sites, those equations influenced by RH and ET showed a larger difference. Understanding the difference in RH and ET between the initial site the model was

calibrated to and the study site discussed here, this aides in better understanding how the model determines $\delta^{18}O_{mod}$.

The most influential and sensitive parameters were found to be RH, the combined factor of $p_{ex}p_x$ and L. The main equations incorporating $p_{ex}p_x$ and L (Equations 3, 4, and 5) are also shown to be sensitive to RH and ET. Other parameters and equations such as T_a, $\delta^{18}O_{wv}$, diffusivity of $H_2{}^{18}O$ in water (D), leaf temperature difference (T_{diff}), concentration of H_2O ([H_2O]), fractionation factors ($\varepsilon_{diff}, \varepsilon_e, \varepsilon_{wc}, \alpha_{ks}, \alpha_{kb}$), leaf internal vapor pressure (e_{leaf}), $^{18}O/^{16}O$ water vapor ($^{18}O/^{16}O_{wv}$), actual vapor pressure of the air (e_{air}), and saturated vapor pressure of the air (e_{sat}) are just as important in determining $\delta^{18}O_{mod}$, but are not influenced by a change in RH or ET from the given study areas. The three most sensitive parameters influence the model by shifting the $\delta^{18}O_{mod}$ along the LMWL as more and less negative values. By understanding that there cannot be a $\delta^{18}O_{mod}$ more negative than the most negative source water, it aides in determining the constraining factors within the model.

6.4 Summer Streamflow Fluctuations

By comparing each individual year of significant summer floods (Figure 1.1) to the $\delta^{18}O_{mod}$ with altered RH, $p_{ex}p_x$, and L parameters (Figure 6.1), assumptions can be made regarding natural functions of the San Pedro river system. As previously stated, summer floods were assumed to be in equilibrium with stream flow for the purposes of this study. While there are many other interactions within the river system, by better understanding the possible correlations of wet versus dry years and the corresponding $\delta^{18}O_{mod}$, potential anthropogenic alterations on the system can be differentiated.

In the years of the lowest summer flooding, the $\delta^{18}O_{mod}$ was generally seen to be more negative (Figure 6.1). The lowest summer flooding years included 1993, 1995, 2002, 2003, and 2009. Looking at the surface water and basin ground water plotted on the LMWL in Figure 4.3, shown in the lower grey shaded line in Figure 6.2, the $\delta^{18}O_{mod}$ during these years corresponded more to the basin ground water with values ranging from -5.58‰ to -10.24‰. It was particularly negative for the Palominas site in 2002 with the most negative outlier value of -10.24‰. Therefore, during some of the lowest years of summer flooding all three sites were relying on basin ground water as source water.

Similarly, in the years of highest streamflow (2006 and 2014), the $\delta^{18}O_{mod}$ was generally more negative, corresponding to the $\delta^{18}O$ basin groundwater range (Figure 6.1). Values of $\delta^{18}O_{mod}$ ranged from -5.20‰ to -9.50‰. This range is more similar to the basin groundwater range than the lowest years of summer flooding, although there is one value which correlated more to stream water. The lowest value at -9.50‰ was in the Lewis Springs site in 2006. The least negative value was in 2014 at the Boquillas site with a value of -5.20‰. This suggests that the Boquillas site is the most sensitive to stream water availability.

Finally, in the years immediately following the highest summer floods (2007 and 2015), there was a correlation between sites. 2007 resulted in overall more negative $\delta^{18}O_{mod}$ with the Palominas site at a value of -10.92‰ and the Boquillas site at the lowest value of -11.44‰. In contrast, 2015 followed the highest summer flooding and was a low flow year, thus resulting in the greatest difference between highest flooding and years following. In 2015, $\delta^{18}O_{mod}$ were less negative, correlating to stream flow. However, 2015 resulted in

the Lewis Springs site with a $\delta^{18}O_{mod}$ value of -0.22‰, the least negative of all $\delta^{18}O_{mod}$ results.

6.5 Future Work and *P. fremontii Reliability*

Given the sensitivity analyses results previously discussed, RH and ET need to be more accurately measureds for each of the study sites. Values for RH and ET gained from a central site is not precise enough. Having this more precise hydroclimatology data will make the model output significantly more accurate.

While the results produced in this study did not determine the degree to which natural function versus human alterations influence the system, it was seen that older *P. fremontii* isotope data is needed from older tree rings. Unfortunately, *Populus* are affected by a rotting fungus, heart rot wood decay (Hickman et al., n.d.), where the center of the tree containing the oldest rigs rots as the tree ages. This makes it difficult to obtain tree rings old enough to compare to a predevelopment period. However, *Prosopis,* more commonly known as Mesquites, do not experience heart rot wood decay, are found in similar environments to *Populus fremontii*, and typically are known to have a deeper root zone than *Populus*. Therefore, this species might be able to show a switch between stream water source and groundwater source easier.

Chapter 7: CONCLUSIONS

Overall, this study has shown the difficulties in modelling source water given isotopic tree ring cellulose, environmental, and atmospheric information. While it can be done with an inversion of the Barbour model (2004) as shown by Sargeant and Singer

(2016), precise environmental and atmospheric data must be known. Therefore, in order to gain modelled source water at these sites, RH must be measured more precisely. There also must be a determination as to whether some parameters should be held constant over time, such as $p_{ex}p_x$, or if they should vary annually at each site. Other species should also be considered such as *Prosopis* which are known to have deeper root zones than the *Populus* and are not seen to be affected by the heart rot wood decay as *Populus* are (Hickman et al., n.d.).

Appendix A: Tables

Site Name	Latitude	Longitude
Palominas	31.36750000	-110.13583333
Lewis Springs	31.56916667	-110.14055556
Boquillas	31.69277778	-110.18722222

Table 2.1 Approximate locations of three study Sites: Palominas (intermittent), Lewis Springs (perennial), and Boquillas (intermittent). Estimated from Google Earth.

Location Name	Latitude	Longitude	Measurement Height	Years of Data
Charleston Mesquite Woodland Site	31.66365	-110.17769	14 m; approx. 5 m above the canopy	2001-2016
Lewis Springs East (Mesquite)	31.56592	-110.13440	7 m; approx. 2 m above canopy	2003-2007; 2012-2016
Lucky Hills (Walnut Gulch)	31.74390	-110.05202	6.2 m; approx. 5 m above canopy	1990-2016

Table 2.2 Locations, measurement heights, and years of data for various flux towers along the San Pedro River (Southwest Watershed Research Center, 2017). After various analyses, due to available data, Lucky Hills was used for all three sites.

Proportion of exchangeable oxygen in cellulose (Roden et la., 1999)	0.42
Proportion of xylem water in meristem (Barbour et al., 2004)	0.8
$^{18}O/^{16}O$ SMOW (Barbour et al., 2004)	0.0020052
Concentration of water (Barbour et al., 2004)	55500 mol m^{-3}
Diffusivity of $H_2{}^{18}O$ in water (Barbour et al., 2004)	$2.66x10^{-9}$ m^2s^{-1}
Diffusive fractionation through stomata (Merlivat et al., 1978)	28 ‰
Diffusive fractionation through boundary layer (Cernusak et al., 2003)	19 ‰
Equilibrium fractionation between C=O and water (Sterberg and DeNiro, 1983)	27 ‰
Leaf temperature difference (Barbour et al., 2004)	1.00 °C

Table 4.3 Model parameter constants across sites and years.

Site	Average Modelled $\delta^{18}O$ Source Water	Average $\delta^{18}O$ Stream Water	$\delta^{18}O_{mod}$ - $\delta^{18}O_{sw}$
Palominas	-9.48	-6.66	-2.82
Lewis Springs	-9.99	-7.60	-2.39
Boquillas	-8.24	-7.20	-1.04

Table 5.1 Average modelled $\delta^{18}O$ source water and average $\delta^{18}O$ stream water for each site.

Appendix B: Figures

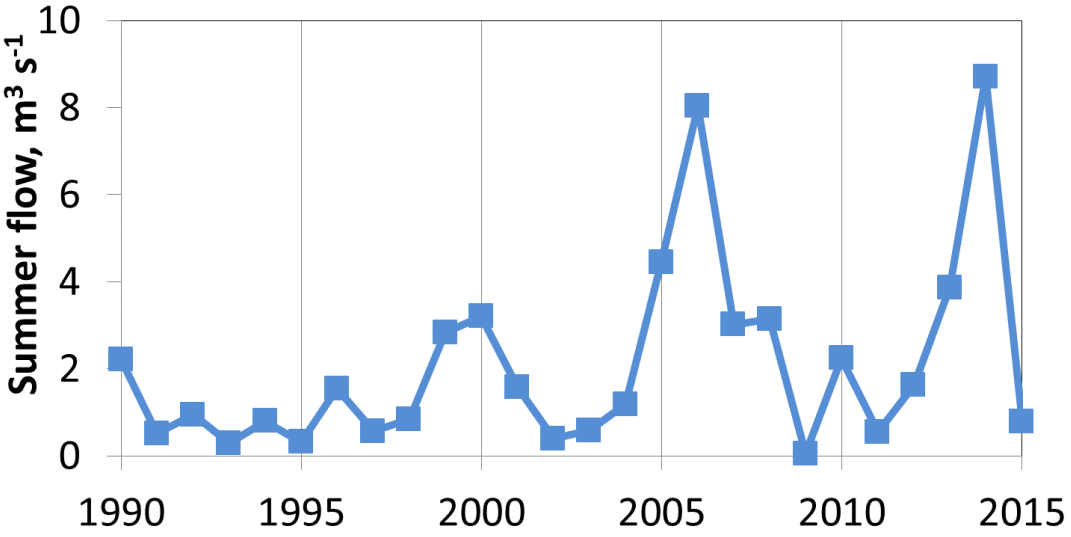

Figure 1.1 Summer (July, August, September) streamflow on the San Pedro River. The three study sites (Palominas, Lewis Springs, and Boquillas) are quite similar in summer flow since most flood flows originate in Mexico and propagate through the full channel network. The period since 1990 has seen highly variable high and low flow summers.

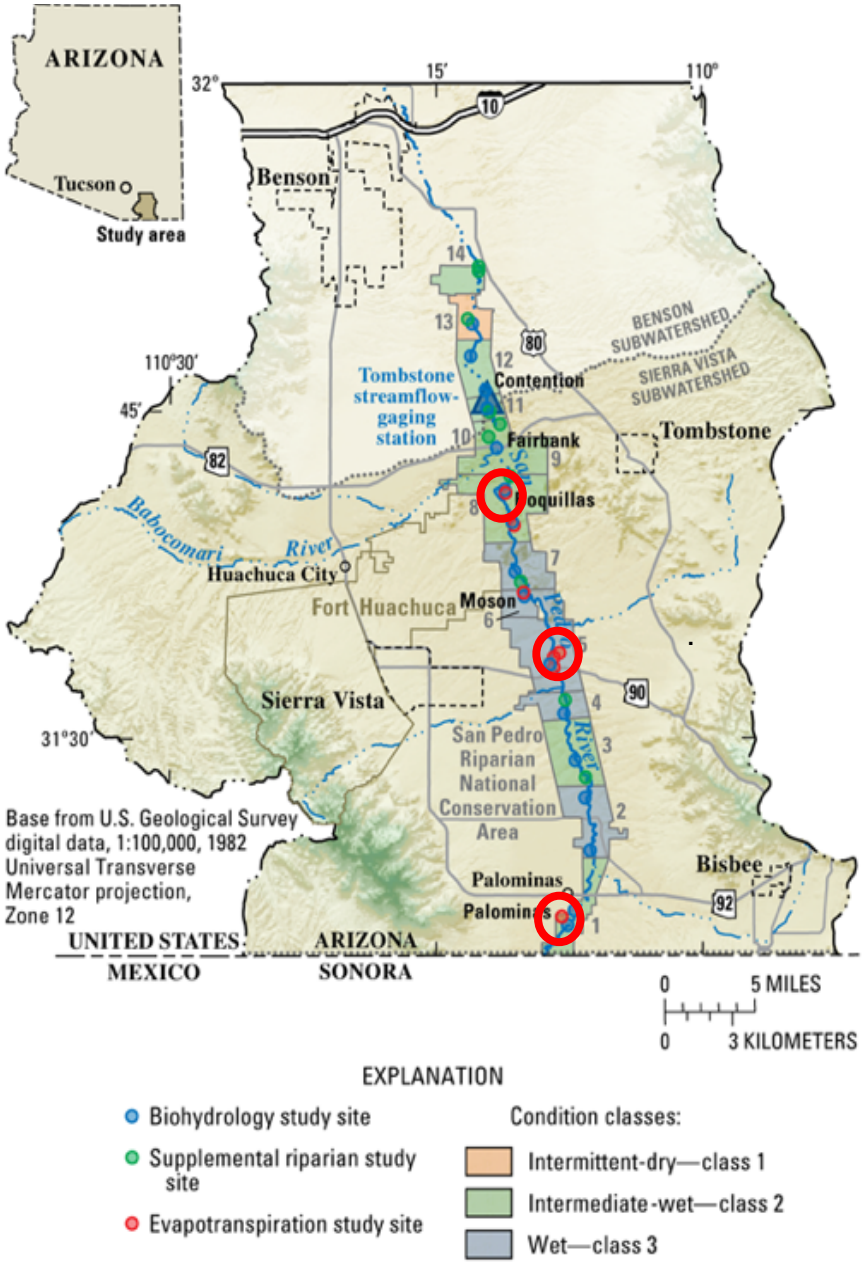

Figure 2.1 Three sites (denoted with red circles): Lewis Springs (perennial), Palominas (intermittent), and Boquillas (intermittent); 16-km N-S transect from Palominas, north to Lewis Springs and Boquillas; (Meixner et al. 2016)

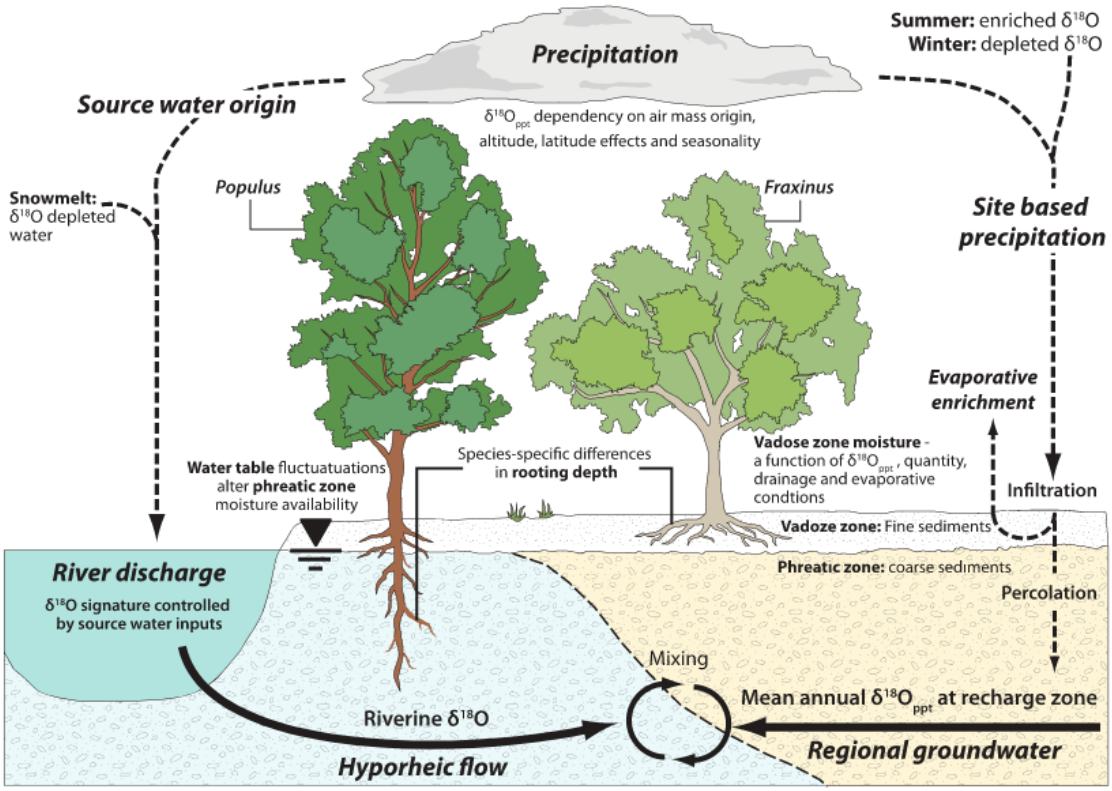

Figure 3.1 Conceptual diagram of isotopic hydrology within the riparian zone along the Rhone River in France. *Populus* and *Fraxinus* were shown to have differing water, identified isotopically (Sargeant and Singer, 2016)

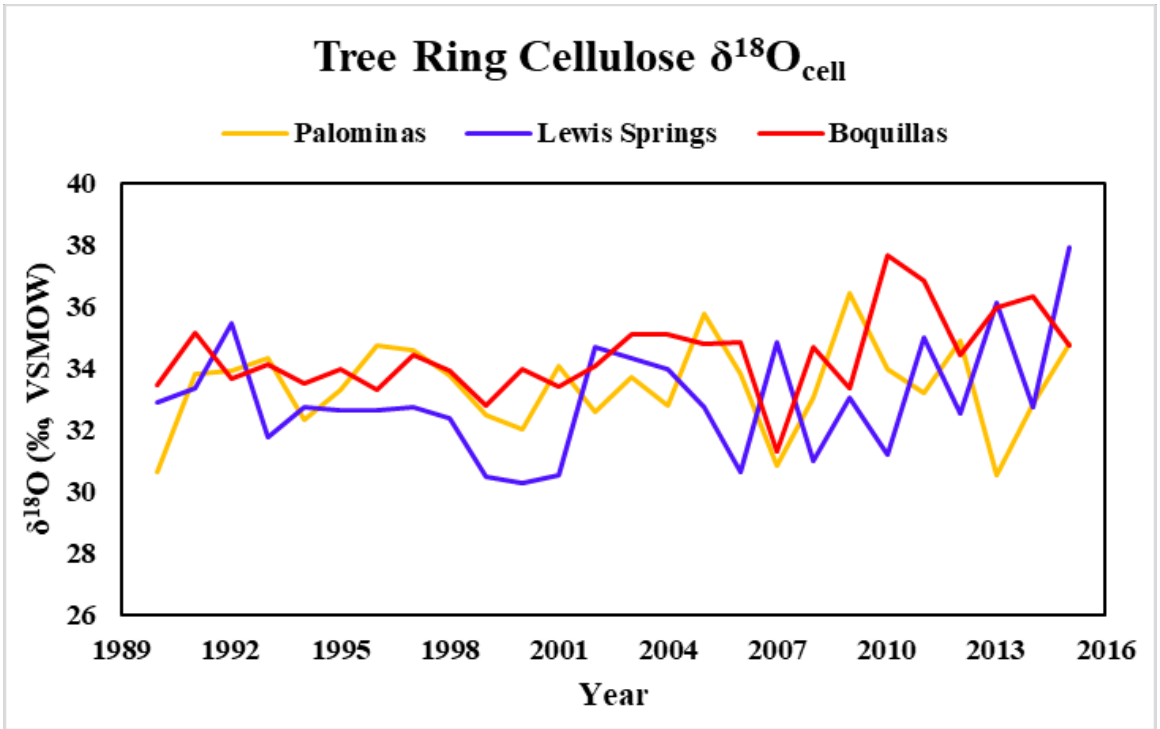

Figure 4.1 Measured tree ring cellulose ($\delta^{18}O_{cell}$) from 1990 to 2016.

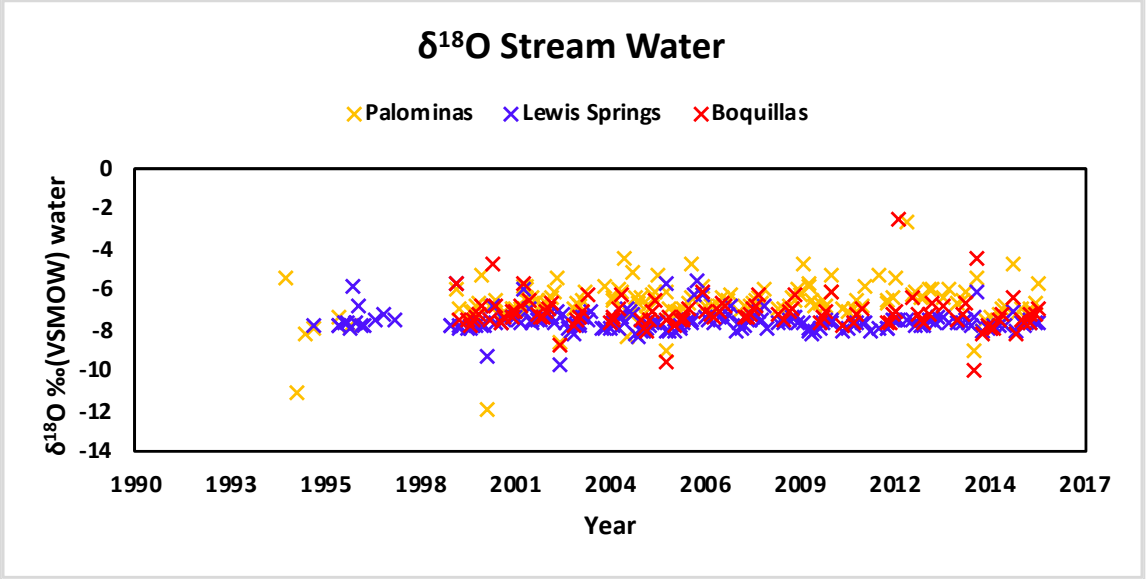

Figure 4.2 Measured $\delta^{18}O$ stream water at the three sites from 1994 through 2016.

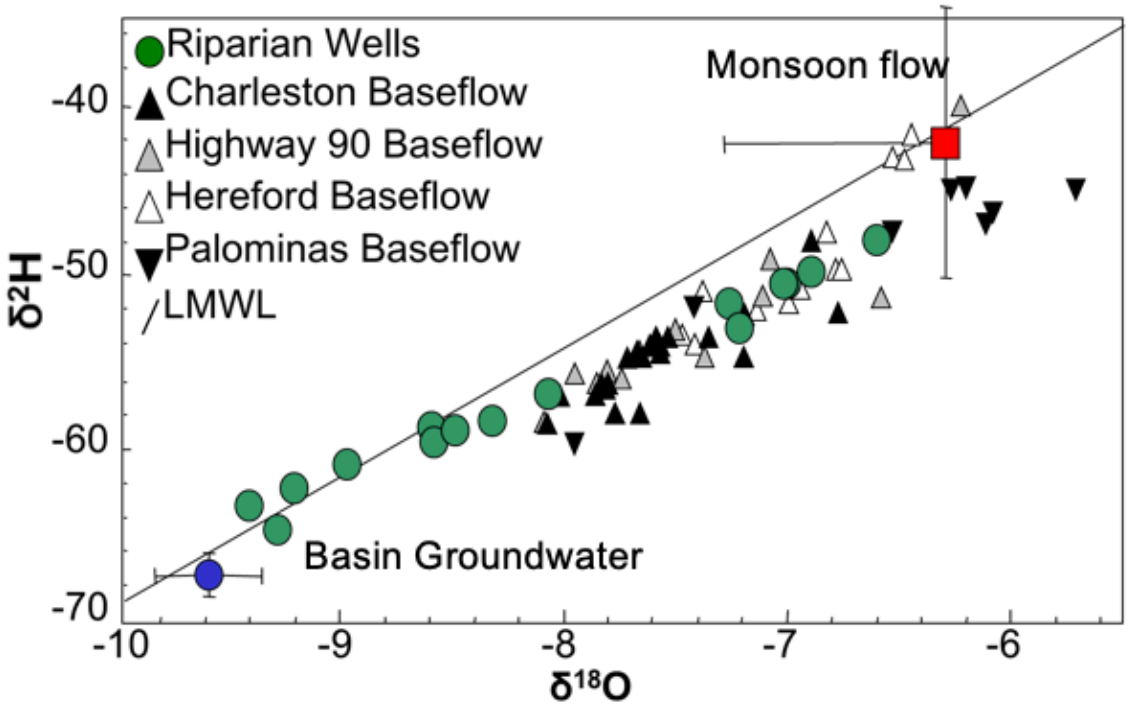

Figure 4.3 Stable isotopes for groundwater and baseflow samples collected from Baillie et al. (2007) and Local Meteoric Water Line (LMWL).

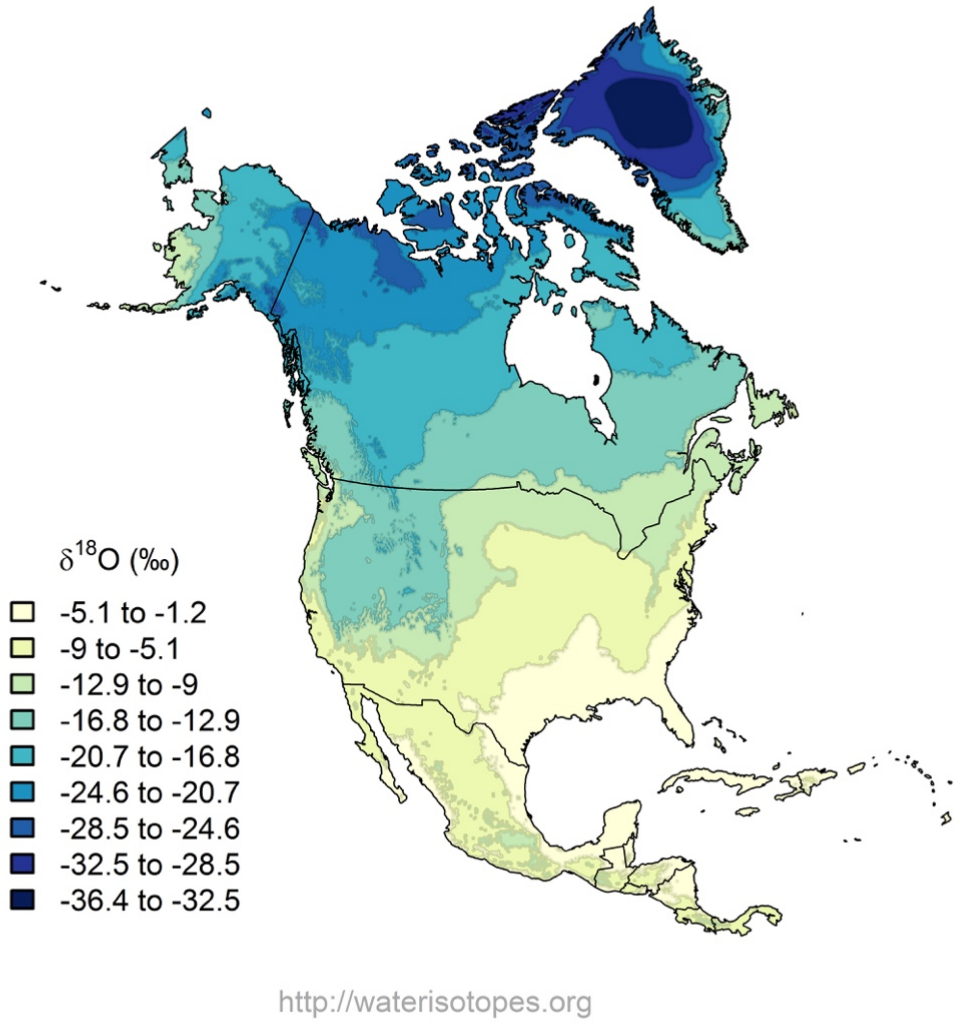

Figure 4.4 North America map of isotope ratios in precipitation, $\delta^{18}O$. The study area is in the color range of -9‰to -5.1‰.

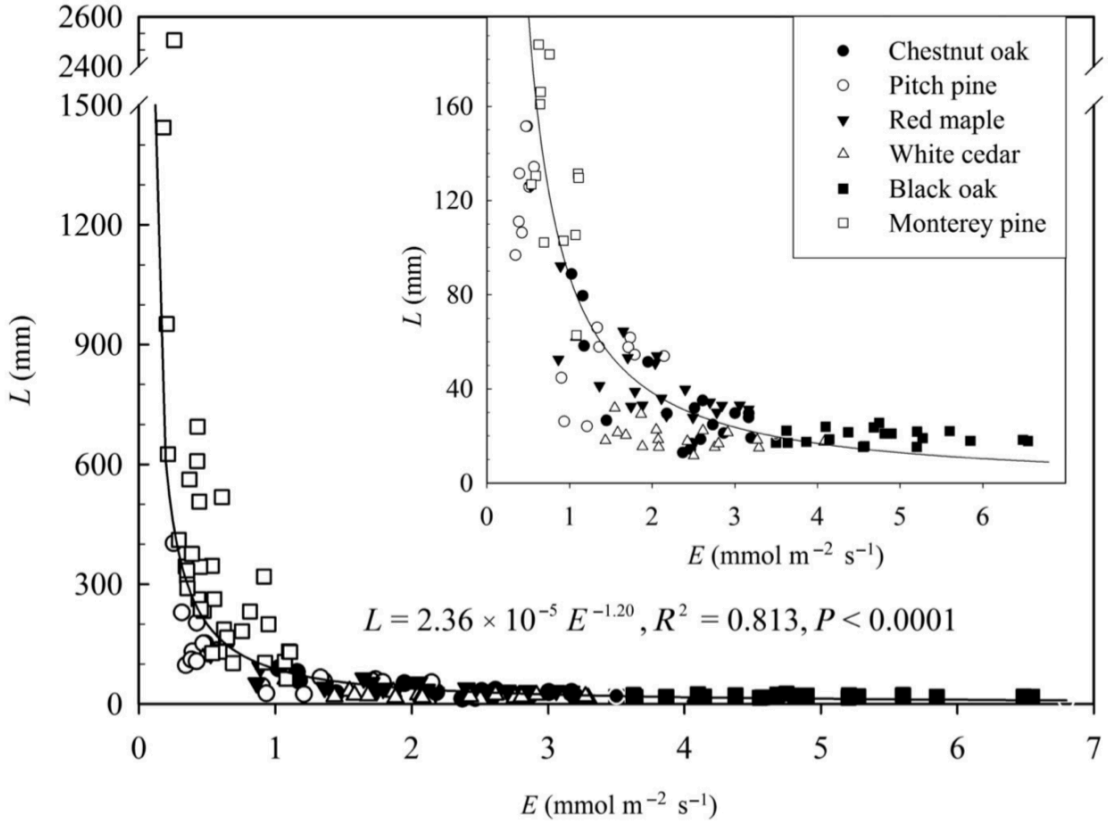

Figure 4.5 "The relationship between effective path length (L) and leaf transpiration rate (E) across all species/sampling periods. The inset is an expansion of the bottom portion of the main graph. Note that the regression function is expressed in Système International units (L in mm and E in mol m^2 s^{-1})." (Song et al., 2013)

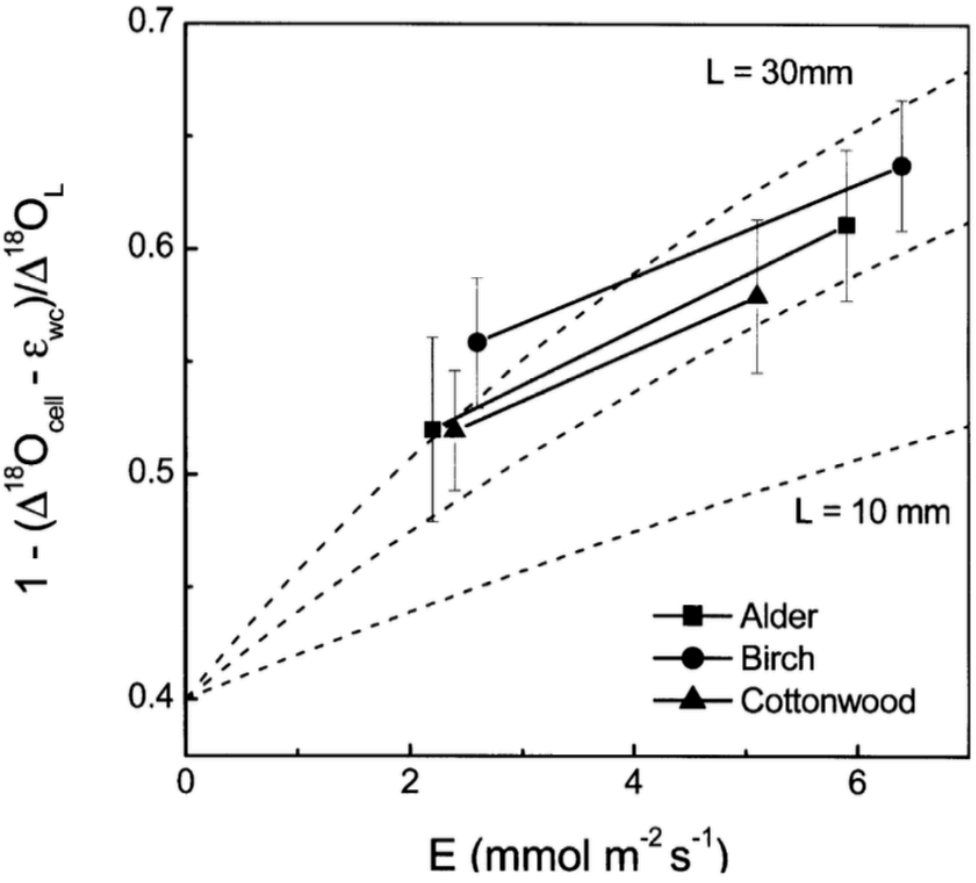

Figure 4.6 "The relationship between evaporation rate and the average fractional difference between $\Delta_{cell}-\varepsilon_{wc}$ [which is the effective water isotopic enrichment in equilibrium with cellulose, and equals $\Delta_L(1-p_{ex}p_x)$] and Craig-Gordon modelled enrichment at the sites of evaporation for three riparian tree species grown at high and low humidity. The predicted relationships at $p_{ex}p_x$=0.40 and effective lengths for the Péclet effect of 10, 20, and 30 mm are plotted as dashed lines. Error bars represent standard errors of the mean values." (Barbour et al., 2004)

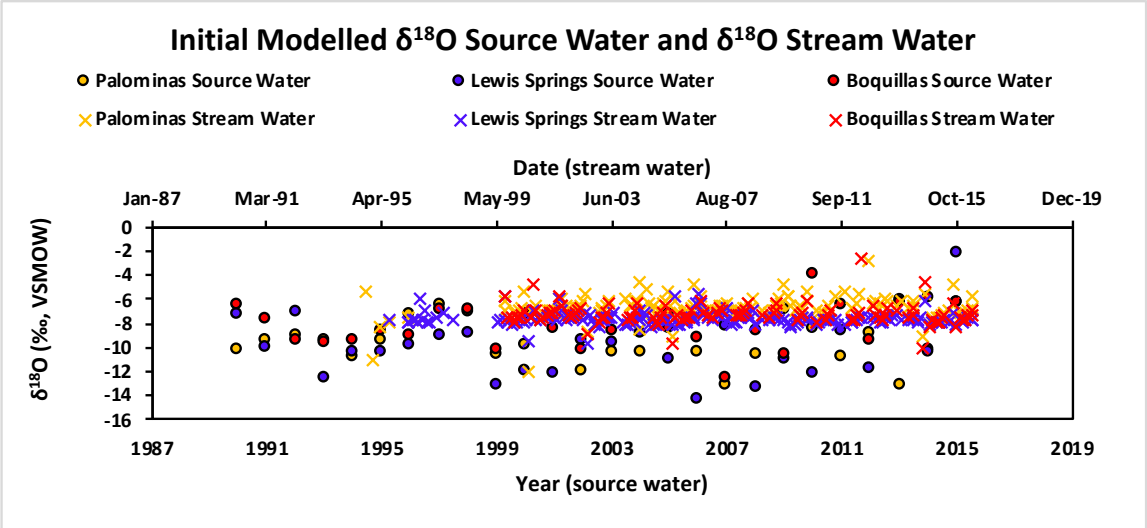

Figure 5.1 Initial $\delta^{18}O_{mod}$ and $\delta^{18}O_{sw}$ for all sites. Circles denote $\delta^{18}O_{mod}$ from 1990 to 2015 and x's denote measured $\delta^{18}O_{sw}$ from approximately 1994 to 2015.

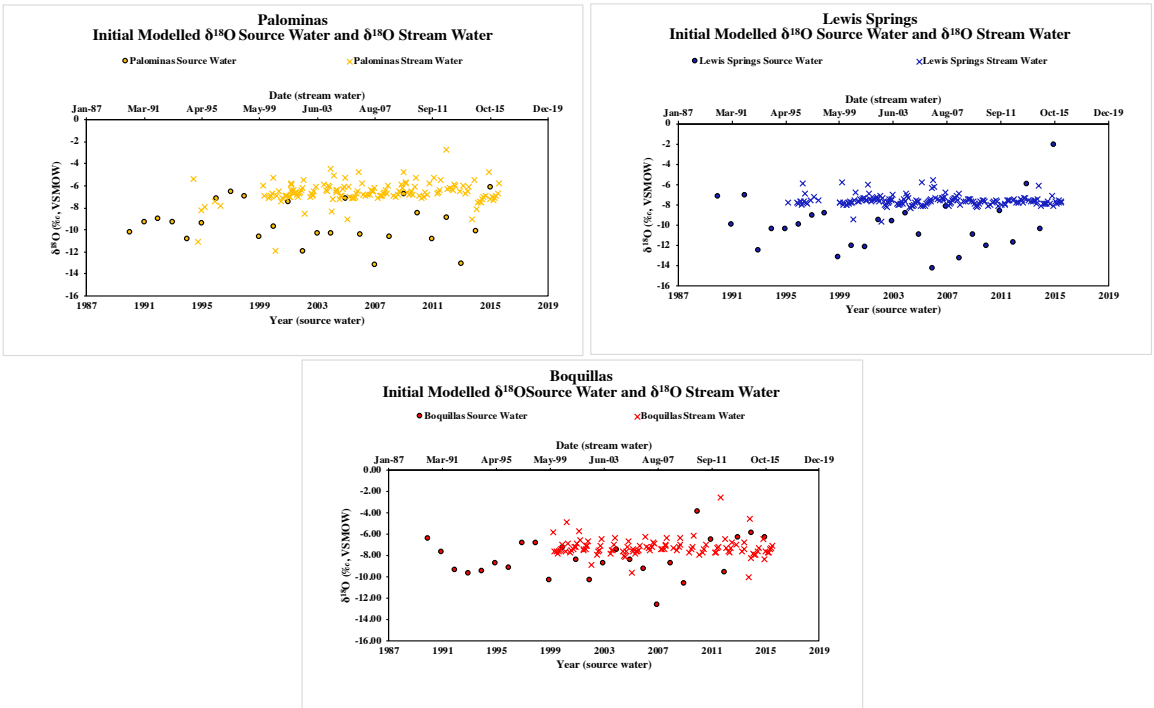

Figure 5.2 Initial $\delta^{18}O_{mod}$ and $\delta^{18}O_{sw}$ for each site. Circles denote $\delta^{18}O_{mod}$ from 1990 to 2015 and x's denote measured $\delta^{18}O_{sw}$ from approximately 1994 to 2015.

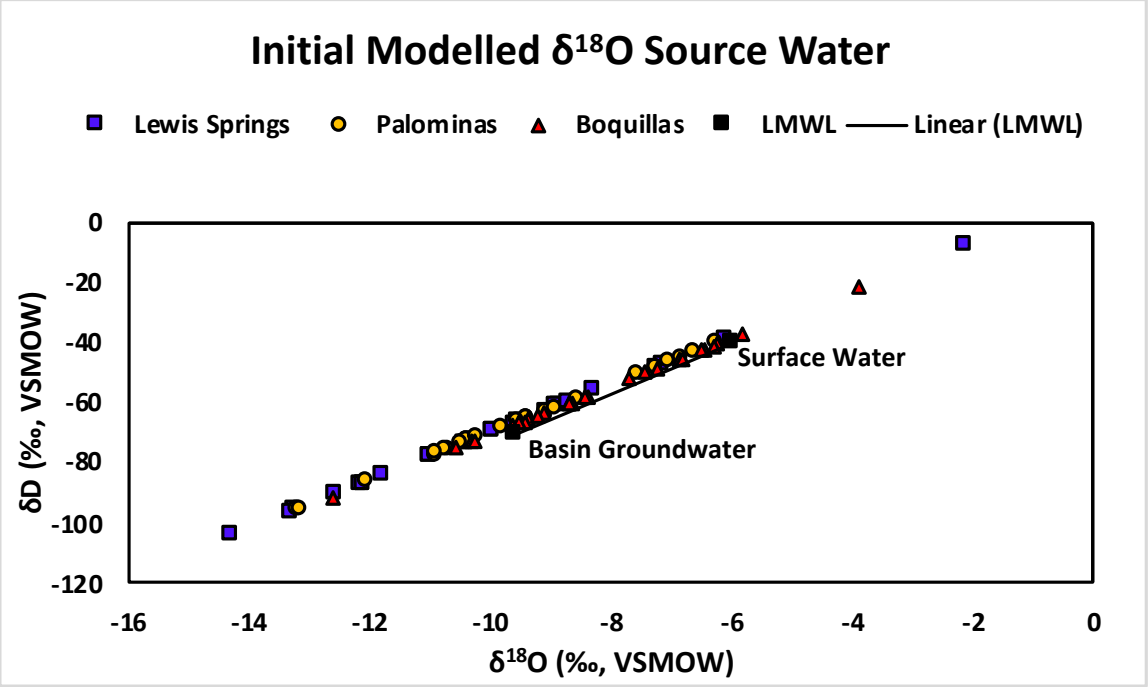

Figure 5.3 Initial $\delta^{18}O_{mod}$ for all sites and Local Meteoric Water Line (LMWL).

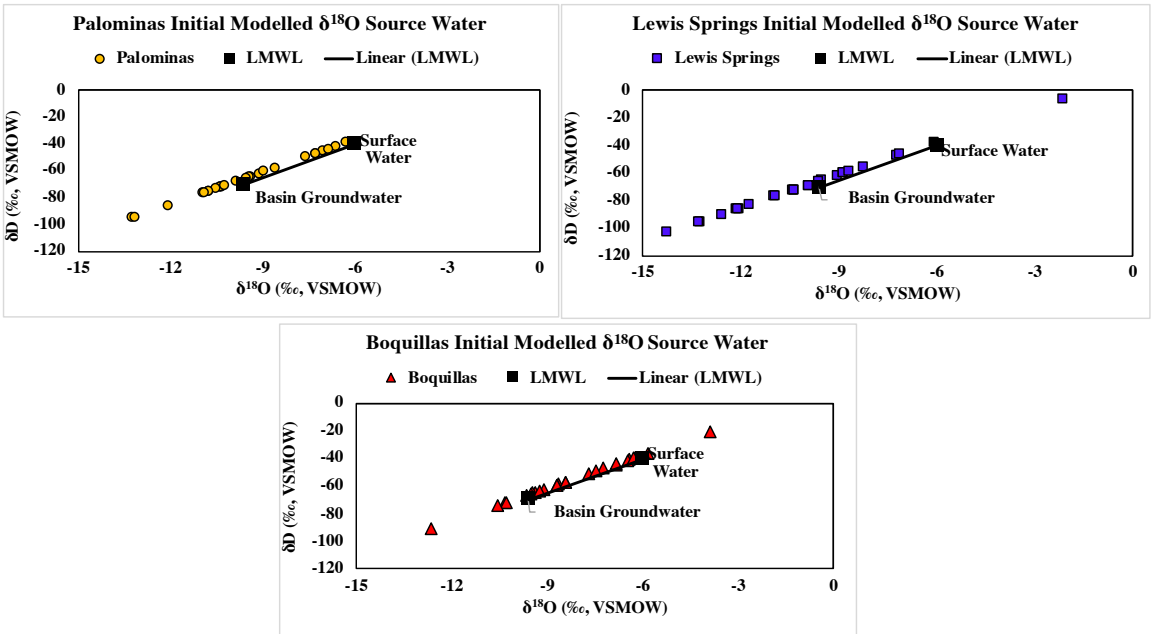

Figure 5.4 Initial $\delta^{18}O_{mod}$ for each sites and Local Meteoric Water Line (LMWL).

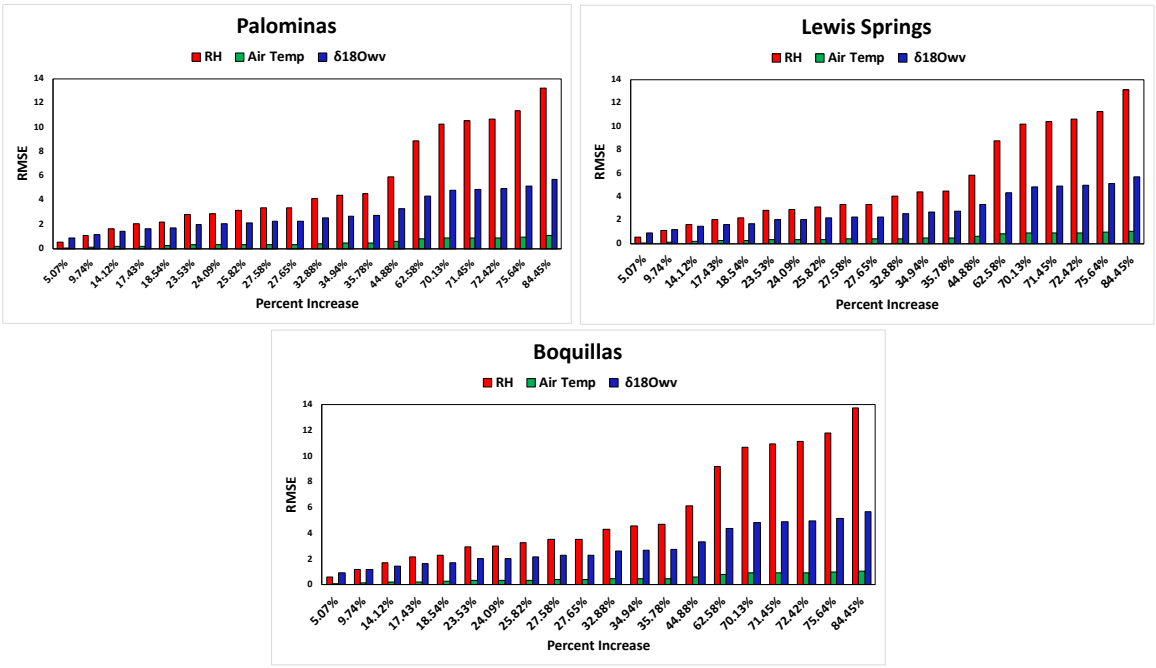

Figure 5.5 Sensitivity Analyses for each site including relative humidity (RH), air temperature, and atmospheric water vapor ($\delta^{18}O_{wv}$).

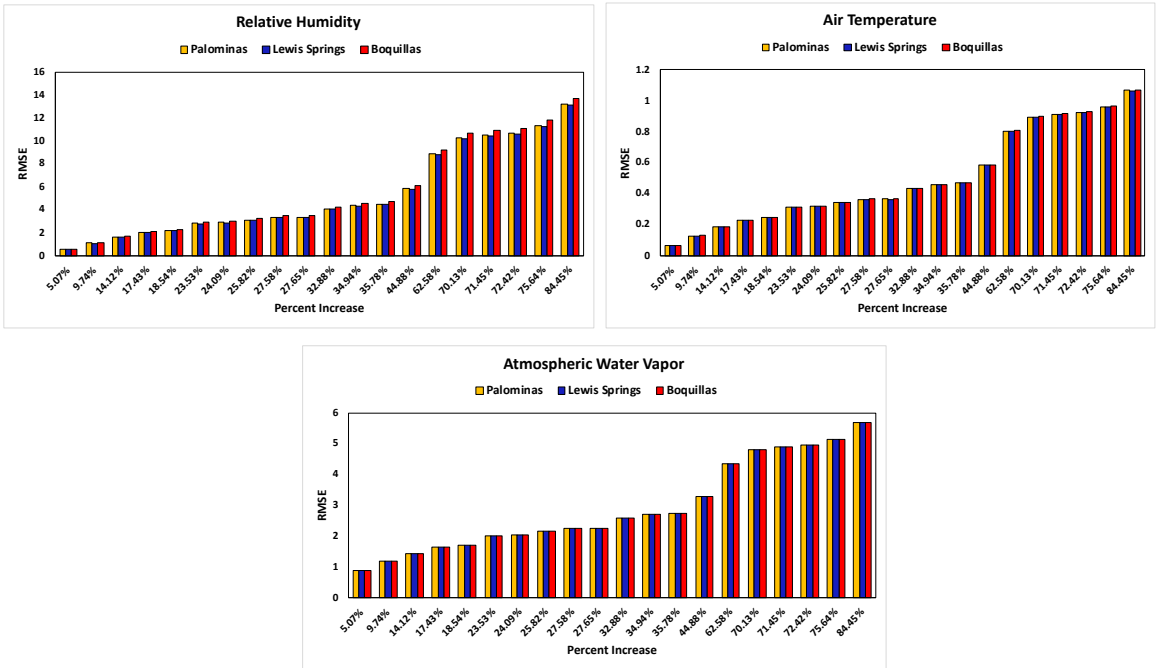

Figure 5.6 Sensitivity Analyses for relative humidity, air temperature, and atmospheric water vapor, all sites.

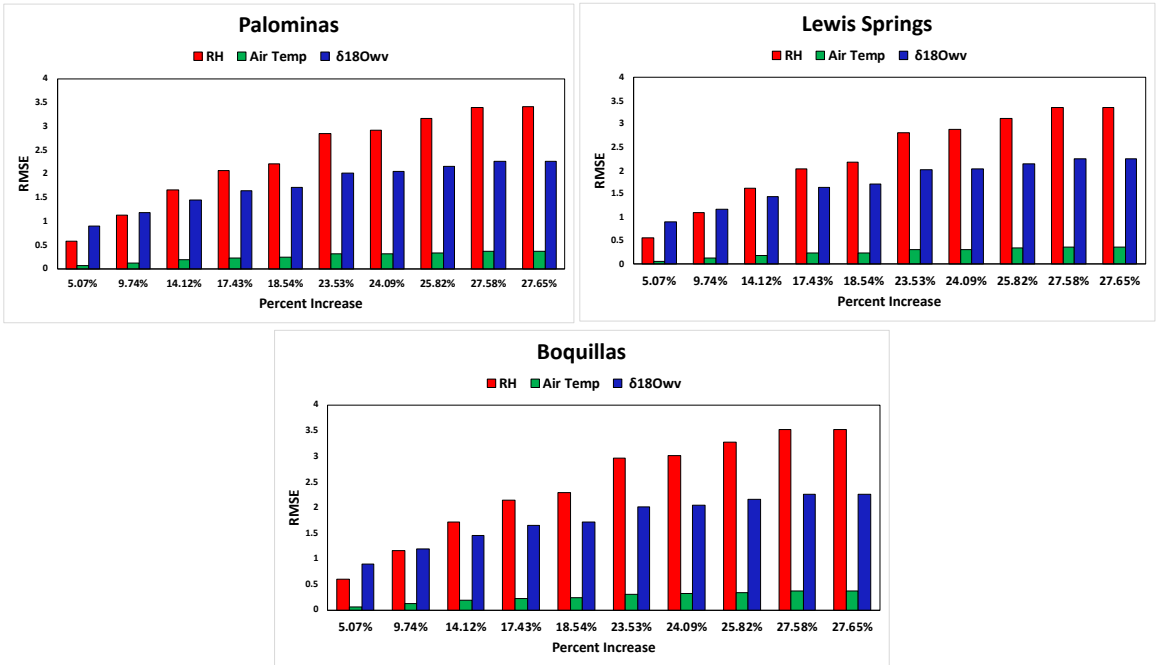

Figure 5.7 Sensitivity Analyses for each site including relative humidity (RH), air temperature, and atmospheric water vapor ($\delta^{18}O_{wv}$), percent increase less than 30%.

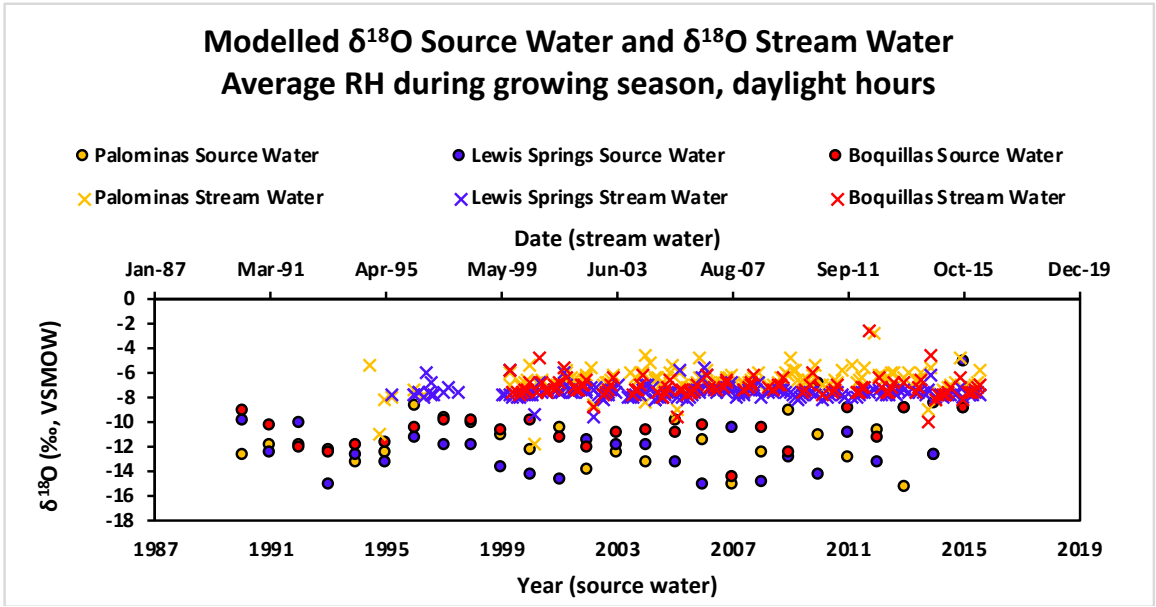

Figure 5.8 $\delta^{18}O_{mod}$ and $\delta^{18}O_{sw}$ for all sites using adjusted RH. Circles denote $\delta^{18}O_{mod}$ from 1990 to 2015 and x's denote measured $\delta^{18}O_{sw}$ from approximately 1994 to 2015.

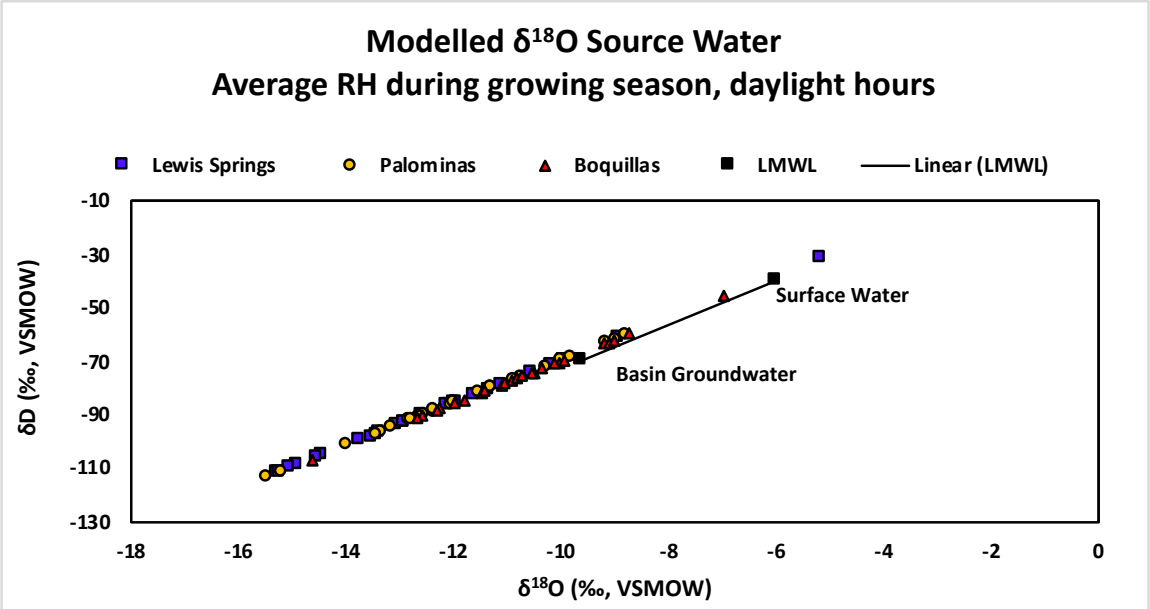

Figure 5.9 $\delta^{18}O_{mod}$ for all sites using adjusted RH and Local Meteoric Water Line (LMWL).

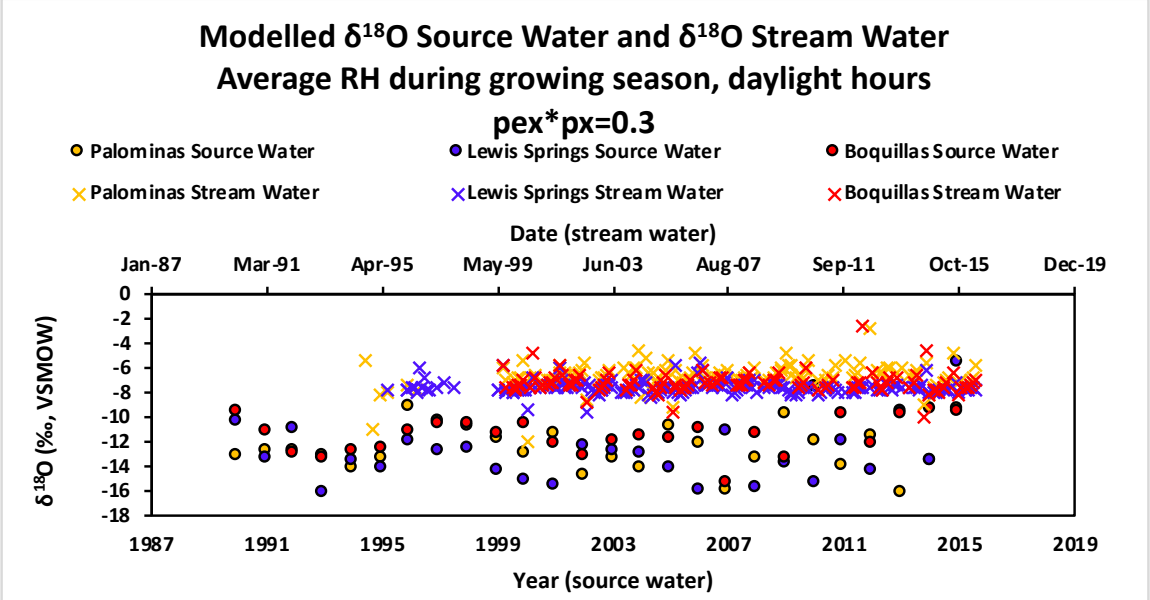

Figure 5.10 $\delta^{18}O_{mod}$ and $\delta^{18}O_{sw}$ for all sites using adjusted RH and combined pex*px = 0.3. Circles denote $\delta^{18}O_{mod}$ from 1990 to 2015 and x's denote measured $\delta^{18}O_{sw}$ from approximately 1994 to 2015.

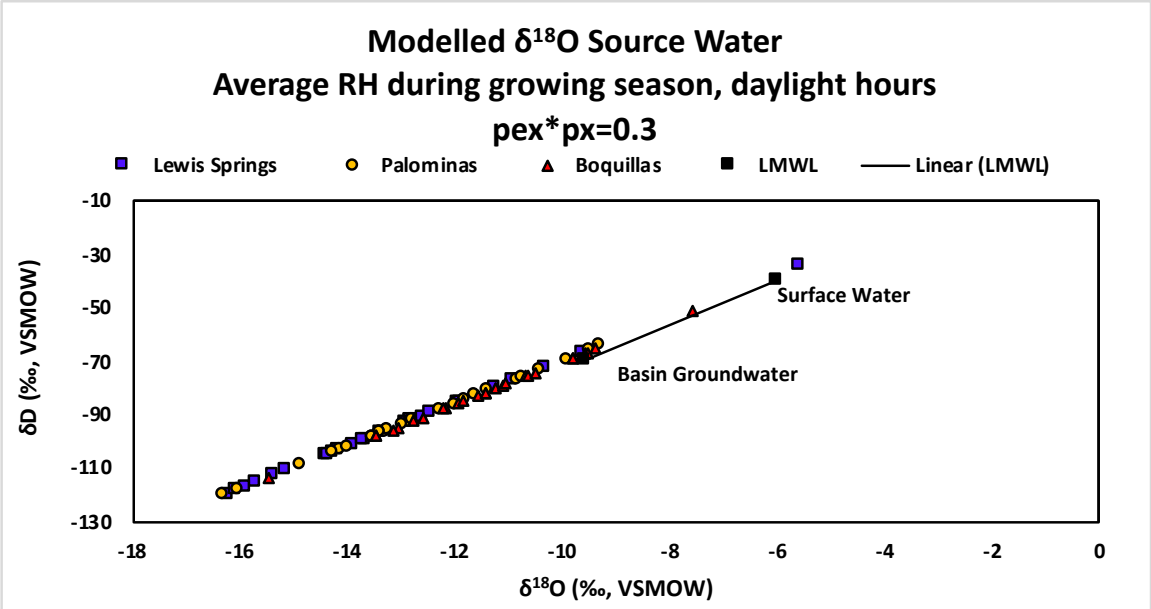

Figure 5.11 $\delta^{18}O_{mod}$ for all sites using adjusted RH, combined pex*px=0.3 and Local Meteoric Water Line (LMWL).

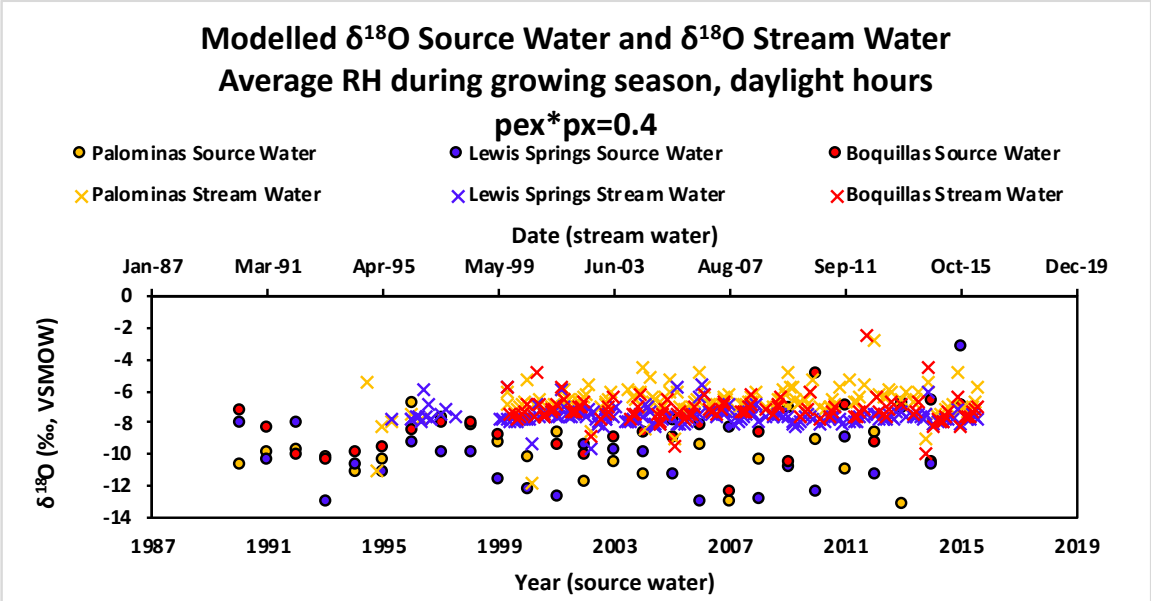

Figure 5.12 $\delta^{18}O_{mod}$ and $\delta^{18}O_{sw}$ for all sites using adjusted RH and combined pex*px = 0.4. Circles denote $\delta^{18}O_{mod}$ from 1990 to 2015 and x's denote measured $\delta^{18}O_{sw}$ from approximately 1994 to 2015.

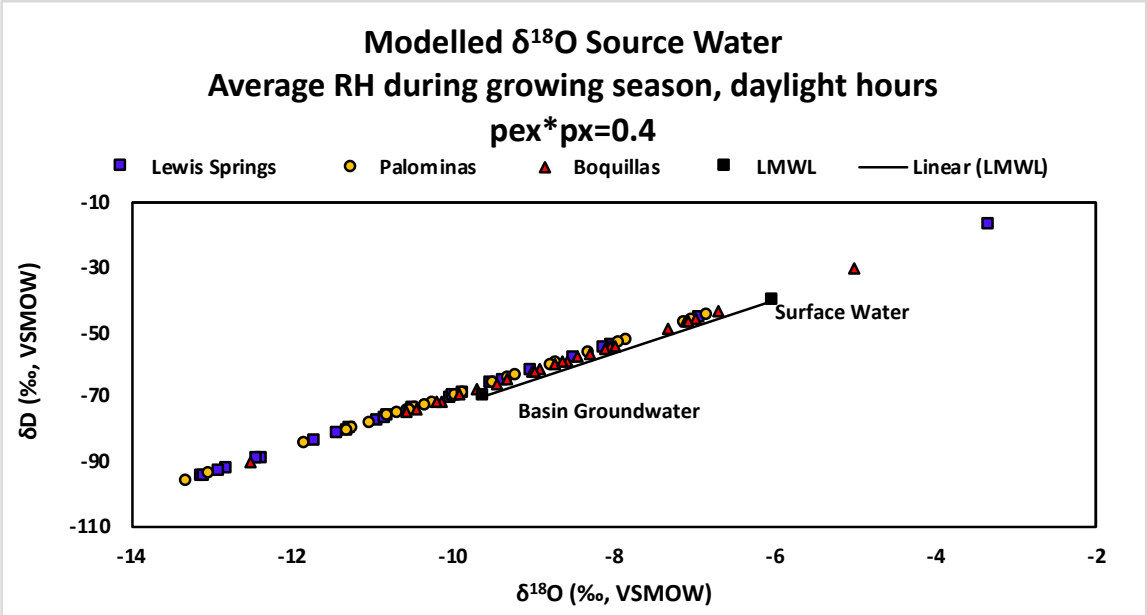

Figure 5.13 $\delta^{18}O_{mod}$ for all sites using adjusted RH, combined pex*px=0.4 and Local Meteoric Water Line (LMWL).

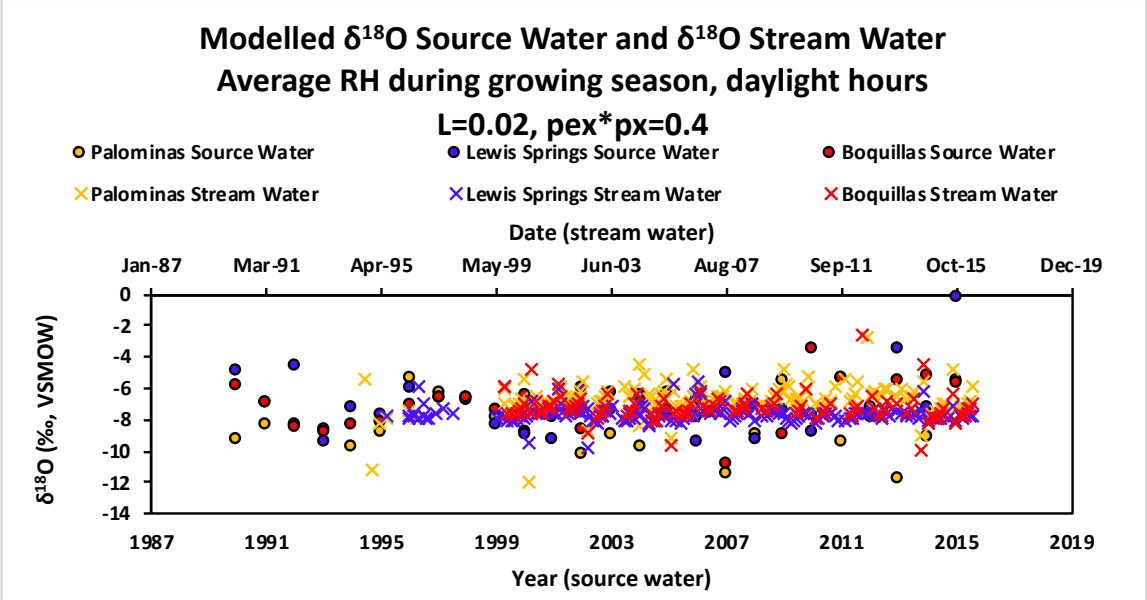

Figure 5.14 $\delta^{18}O_{mod}$ and $\delta^{18}O_{sw}$ for all sites using adjusted RH and combined pex*px = 0.4 and L=0.02 m. Circles denote $\delta^{18}O_{mod}$ from 1990 to 2015 and x's denote measured $\delta^{18}O_{sw}$ from approximately 1994 to 2015.

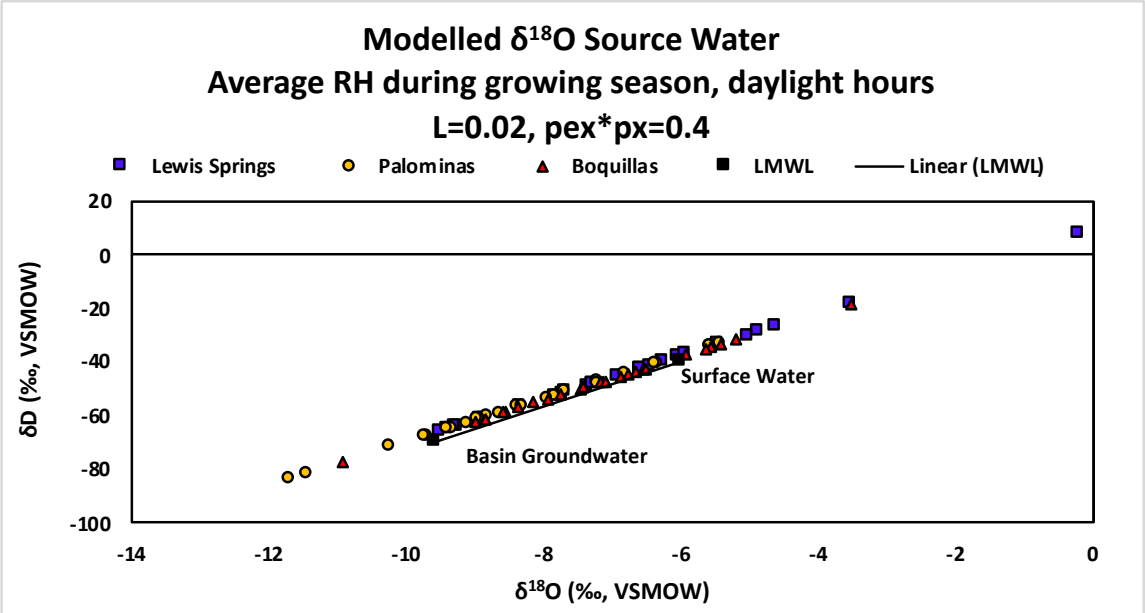

Figure 5.15 $\delta^{18}O_{mod}$ for all sites using adjusted RH, combined pex*px=0.4, L=0.02 m, and Local Meteoric Water Line (LMWL).

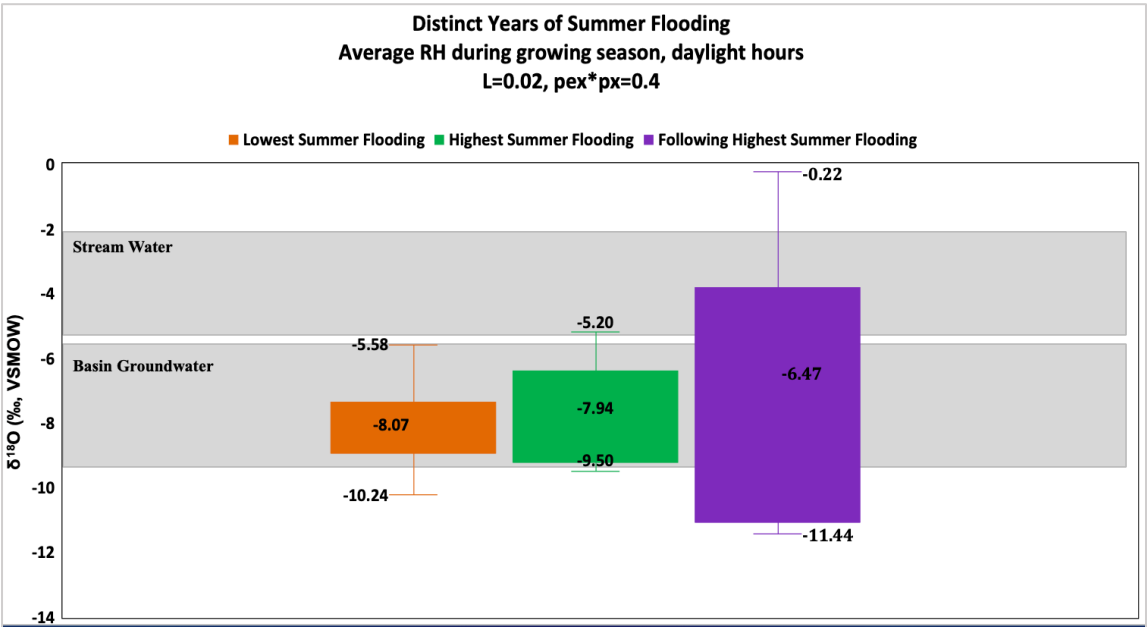

Figure 6.1 Distinct years of summer flooding using average RH values during the growing season and daylight hours only as well as the adjusted $p_{ex}p_x$ value of 0.4 and the adjusted L value of 0.02 m.

Appendix C: Statistical Results

Anova: Single Factor

SUMMARY

Groups	*Count*	*Sum*	*Average*	*Variance*
P	149	-991.95	-6.65738255	0.95964918
LS	149	-1131.4	-7.59328859	0.27376546
B	107	-769.97	-7.19598131	0.71345823

ANOVA

Source of Variation	*SS*	*df*	*MS*	*F*	*P-value*	*F crit*
Between Groups	65.6489803	2	32.8244901	51.1110737	1.6689E-20	3.018168
Within Groups	258.17194	402	0.64221876			
Total	323.82092	404				

Figure 1 ANOVA test for stream water locations ($\delta^{18}O_{sw}$). Palominas (P), Lewis Springs (LS), Boquillas (B). Significantly different.

Anova: Single Factor

SUMMARY

Groups	*Count*	*Sum*	*Average*	*Variance*
P	26	869.5442	33.44401	2.108566
LS	26	858.7553	33.02905	3.552128
B	26	895.1718	34.42968	1.732181

ANOVA

Source of Variation	*SS*	*df*	*MS*	*F*	*P-value*	*F crit*
Between Groups	26.91456	2	13.45728	5.460913	0.006108	3.118642
Within Groups	184.8219	75	2.464292			
Total	211.7364	77				

Figure 2 ANOVA test for tree ring cellulose at each of the locations ($\delta^{18}O_{cell}$). Palominas (P), Lewis Springs (LS), Boquillas (B). Significantly different.

Low

Anova: Single Factor

SUMMARY

Groups	*Count*	*Sum*	*Average*	*Variance*
P	26	-262.820066	-10.1084641	3.54819921
LS	26	-276.124111	-10.6201581	6.49883983
B	26	-230.470863	-8.86426397	3.30774645

ANOVA

Source of Variation	*SS*	*df*	*MS*	*F*	*P-value*	*F crit*
Between Groups	42.4062501	2	21.2031251	4.76303983	0.01128873	3.11864213
Within Groups	333.869637	75	4.45159516			
Total	376.275887	77				

Average

Anova: Single Factor

SUMMARY

Groups	*Count*	*Sum*	*Average*	*Variance*
P	26	-246.54255	-9.48240578	3.66243344
LS	26	-259.846327	-9.9940895	6.66602436
B	26	-214.193348	-8.23820569	3.46324623

ANOVA

Source of Variation	*SS*	*df*	*MS*	*F*	*P-value*	*F crit*
Between Groups	42.4058447	2	21.2029223	4.61210354	0.01290959	3.11864213
Within Groups	344.792601	75	4.59723467			
Total	387.198445	77				

High

Anova: Single Factor

SUMMARY

Groups	*Count*	*Sum*	*Average*	*Variance*
P	26	-231.078911	-8.88765041	3.78536289
LS	26	-244.382433	-9.39932434	6.83925723
B	26	-198.729708	-7.64345031	3.62537797

ANOVA

Source of Variation	*SS*	*df*	*MS*	*F*	*P-value*	*F crit*
Between Groups	42.40546	2	21.20273	4.46373322	0.01473646	3.11864213
Within Groups	356.249952	75	4.74999936			
Total	398.655412	77				

Figure 3 ANOVA test for field site locations ($\delta^{18}O_{mod}$). Palominas (P), Lewis Springs (LS), Boquillas (B). Low $\delta^{18}O_{wv}$ (Low), Average $\delta^{18}O_{wv}$ (Average), High $\delta^{18}O_{wv}$ (High). Significantly different.

Anova: Single Factor

SUMMARY

Groups	Count	Sum	Average	Variance
P Low	26	-262.820066	-10.1084641	3.54819921
P Average	26	-246.54255	-9.48240578	3.66243344
P High	26	-231.078911	-8.88765041	3.78536289

ANOVA

Source of Variation	SS	df	MS	F	P-value	F crit
Between Groups	19.3792642	2	9.68963212	2.64358932	0.07772576	3.11864213
Within Groups	274.899888	75	3.66533185			
Total	294.279153	77				

Anova: Single Factor

SUMMARY

Groups	Count	Sum	Average	Variance
LS Low	26	-276.124111	-10.6201581	6.49883983
LS Average	26	-259.846327	-9.9940895	6.66602436
LS High	26	-244.382433	-9.39932434	6.83925723

ANOVA

Source of Variation	SS	df	MS	F	P-value	F crit
Between Groups	19.3799023	2	9.68995117	1.45319321	0.24032979	3.11864213
Within Groups	500.103036	75	6.66804047			
Total	519.482938	77				

Anova: Single Factor

SUMMARY

Groups	Count	Sum	Average	Variance
B Low	26	-230.470863	-8.86426397	3.30774645
B Average	26	-214.193348	-8.23820569	3.46324623
B High	26	-198.729708	-7.64345031	3.62537797

ANOVA

Source of Variation	SS	df	MS	F	P-value	F crit
Between Groups	19.3792641	2	9.68963205	2.79606193	0.0674256	3.11864213
Within Groups	259.909266	75	3.46545688			
Total	279.28853	77				

Figure 4 ANOVA test for each field site location ($\delta^{18}O_{mod}$). Palominas (P), Lewis Springs (LS), Boquillas (B). Low $\delta^{18}O_{wv}$ (Low), Average $\delta^{18}O_{wv}$ (Average), High $\delta^{18}O_{wv}$ (High). Not significantly different.

	Palominas		
Low	t-Test: Two-Sample Assuming Unequal Variances		
		Variable 1	*Variable 2*
	Mean	-6.65738255	-10.1084641
	Variance	0.95964918	3.54819921
	Observations	149	26
	Hypothesized Mean Difference	0	
	df	27	
	t Stat	9.12902118	
	P(T<=t) one-tail	4.8304E-10	
	t Critical one-tail	1.70328845	
	P(T<=t) two-tail	9.6608E-10	
	t Critical two-tail	2.05183052	
Average	t-Test: Two-Sample Assuming Unequal Variances		
		Variable 1	*Variable 2*
	Mean	-6.65738255	-9.48240578
	Variance	0.95964918	3.66243344
	Observations	149	26
	Hypothesized Mean Difference	0	
	df	27	
	t Stat	7.36064045	
	P(T<=t) one-tail	3.2192E-08	
	t Critical one-tail	1.70328845	
	P(T<=t) two-tail	6.4384E-08	
	t Critical two-tail	2.05183052	
High	t-Test: Two-Sample Assuming Unequal Variances		
		Variable 1	*Variable 2*
	Mean	-6.65738255	-8.88765041
	Variance	0.95964918	3.78536289
	Observations	149	26
	Hypothesized Mean Difference	0	
	df	27	
	t Stat	5.71992409	
	P(T<=t) one-tail	2.2196E-06	
	t Critical one-tail	1.70328845	
	P(T<=t) two-tail	4.4392E-06	
	t Critical two-tail	2.05183052	

Figure 5 T-test for Palominas field site location ($\delta^{18}O_{mod}$) against Palominas stream water ($\delta^{18}O_{sw}$). Low $\delta^{18}O_{wv}$ (Low), Average $\delta^{18}O_{wv}$ (Average), High $\delta^{18}O_{wv}$ (High). Significantly different.

	Lewis Springs		
Low	t-Test: Two-Sample Assuming Unequal Variances		
		Variable 1	*Variable 2*
	Mean	-7.59785311	-10.6201581
	Variance	0.25074991	6.49883983
	Observations	177	26
	Hypothesized Mean Difference	0	
	df	25	
	t Stat	6.02809101	
	P(T<=t) one-tail	1.3441E-06	
	t Critical one-tail	1.70814076	
	P(T<=t) two-tail	2.6883E-06	
	t Critical two-tail	2.05953855	
Average	t-Test: Two-Sample Assuming Unequal Variances		
		Variable 1	*Variable 2*
	Mean	-7.59785311	-9.9940895
	Variance	0.25074991	6.66602436
	Observations	177	26
	Hypothesized Mean Difference	0	
	df	25	
	t Stat	4.71939507	
	P(T<=t) one-tail	3.8553E-05	
	t Critical one-tail	1.70814076	
	P(T<=t) two-tail	7.7106E-05	
	t Critical two-tail	2.05953855	
High	t-Test: Two-Sample Assuming Unequal Variances		
		Variable 1	*Variable 2*
	Mean	-7.59785311	-9.39932434
	Variance	0.25074991	6.83925723
	Observations	177	26
	Hypothesized Mean Difference	0	
	df	25	
	t Stat	3.50302479	
	P(T<=t) one-tail	0.00087608	
	t Critical one-tail	1.70814076	
	P(T<=t) two-tail	0.00175215	
	t Critical two-tail	2.05953855	

Figure 6 T-test for Lewis Springs field site location ($\delta^{18}O_{mod}$) against Lewis Springs stream water ($\delta^{18}O_{sw}$). Low $\delta^{18}O_{wv}$ (Low), Average $\delta^{18}O_{wv}$ (Average), High $\delta^{18}O_{wv}$ (High). Significantly different.

	Boquillas		
Low	t-Test: Two-Sample Assuming Unequal Variances		
		Variable 1	*Variable 2*
	Mean	-7.19598131	-8.86426397
	Variance	0.71345823	3.30774645
	Observations	107	26
	Hypothesized Mean Difference	0	
	df	28	
	t Stat	4.55929223	
	P(T<=t) one-tail	4.6223E-05	
	t Critical one-tail	1.70113093	
	P(T<=t) two-tail	9.2446E-05	
	t Critical two-tail	2.04840714	
Average	t-Test: Two-Sample Assuming Unequal Variances		
		Variable 1	*Variable 2*
	Mean	-7.19598131	-8.23820569
	Variance	0.71345823	3.46324623
	Observations	107	26
	Hypothesized Mean Difference	0	
	df	28	
	t Stat	2.78675984	
	P(T<=t) one-tail	0.00472579	
	t Critical one-tail	1.70113093	
	P(T<=t) two-tail	0.00945158	
	t Critical two-tail	2.04840714	
High	t-Test: Two-Sample Assuming Unequal Variances		
		Variable 1	*Variable 2*
	Mean	-7.19598131	-7.64345031
	Variance	0.71345823	3.62537797
	Observations	107	26
	Hypothesized Mean Difference	0	
	df	27	
	t Stat	1.17065723	
	P(T<=t) one-tail	0.12598277	
	t Critical one-tail	1.70328845	
	P(T<=t) two-tail	0.25196555	
	t Critical two-tail	2.05183052	

Figure 7 T-test for Boquillas field site location ($\delta^{18}O_{mod}$) against Boquillas stream water ($\delta^{18}O_{sw}$). Low $\delta^{18}O_{wv}$ (Low), Average $\delta^{18}O_{wv}$ (Average), High $\delta^{18}O_{wv}$ (High). Significantly different except for Boquillas High which is not significantly different.

Palominas	t-Test: Two-Sample Assuming Unequal Variances		
		Variable 1	*Variable 2*
	Mean	-6.57971	-9.83299
	Variance	0.141967	4.1927
	Observations	17	17
	Hypothesized Mean Difference	0	
	df	17	
	t Stat	6.442709	
	P(T<=t) one-tail	3.04E-06	
	t Critical one-tail	1.739607	
	P(T<=t) two-tail	6.07E-06	
	t Critical two-tail	2.109816	
Lewis Springs	t-Test: Two-Sample Assuming Unequal Variances		
		Variable 1	*Variable 2*
	Mean	-7.603	-10.2539
	Variance	0.032417	8.782494
	Observations	17	17
	Hypothesized Mean Difference	0	
	df	16	
	t Stat	3.681354	
	P(T<=t) one-tail	0.00101	
	t Critical one-tail	1.745884	
	P(T<=t) two-tail	0.00202	
	t Critical two-tail	2.119905	
Boquillas	t-Test: Two-Sample Assuming Unequal Variances		
		Variable 1	*Variable 2*
	Mean	-7.17019	-8.23821
	Variance	0.09142	3.463246
	Observations	17	26
	Hypothesized Mean Difference	0	
	df	27	
	t Stat	2.868992	
	P(T<=t) one-tail	0.003951	
	t Critical one-tail	1.703288	
	P(T<=t) two-tail	0.007902	
	t Critical two-tail	2.051831	

Figure 8 T-tests for each field site location ($\delta^{18}O_{mod}$) against each site stream water ($\delta^{18}O_{sw}$), respectively. Using the average $\delta^{18}O_{wv}$. All significantly different.

Palominas	t-Test: Two-Sample Assuming Unequal Variances		
		Variable 1	*Variable 2*
	Mean	2.38330754	33.5579696
	Variance	6.03676269	2.21435173
	Observations	20	20
	Hypothesized Mean Difference	0	
	df	31	
	t Stat	-48.535605	
	P(T<=t) one-tail	4.1174E-31	
	t Critical one-tail	1.69551878	
	P(T<=t) two-tail	8.2347E-31	
	t Critical two-tail	2.03951345	
Lewis Springs	t-Test: Two-Sample Assuming Unequal Variances		
		Variable 1	*Variable 2*
	Mean	2.08749743	33.0290489
	Variance	4.89366562	3.55212768
	Observations	26	26
	Hypothesized Mean Difference	0	
	df	49	
	t Stat	-54.288587	
	P(T<=t) one-tail	9.7876E-46	
	t Critical one-tail	1.67655089	
	P(T<=t) two-tail	1.9575E-45	
	t Critical two-tail	2.00957524	
Boquillas	t-Test: Two-Sample Assuming Unequal Variances		
		Variable 1	*Variable 2*
	Mean	2.62841009	34.5236907
	Variance	6.2396515	2.24742662
	Observations	19	19
	Hypothesized Mean Difference	0	
	df	29	
	t Stat	-47.722603	
	P(T<=t) one-tail	2.0447E-29	
	t Critical one-tail	1.69912703	
	P(T<=t) two-tail	4.0894E-29	
	t Critical two-tail	2.04522964	

Figure 9 T-tests for each field site location ($\delta^{18}O_{mod}$) against each site stream water flow (m^3/s^2), respectively. Using the average $\delta^{18}O_{wv}$. All significantly different.

Palominas	t-Test: Two-Sample Assuming Unequal Variances		
		Variable 1	*Variable 2*
	Mean	2.38330754	-9.4000979
	Variance	6.03676269	4.65991143
	Observations	20	20
	Hypothesized Mean Difference	0	
	df	37	
	t Stat	16.1124446	
	P(T<=t) one-tail	1.3107E-18	
	t Critical one-tail	1.68709362	
	P(T<=t) two-tail	2.6214E-18	
	t Critical two-tail	2.02619246	
Lewis Springs	t-Test: Two-Sample Assuming Unequal Variances		
		Variable 1	*Variable 2*
	Mean	2.08749743	-9.9940895
	Variance	4.89366562	6.66602436
	Observations	26	26
	Hypothesized Mean Difference	0	
	df	49	
	t Stat	18.1191393	
	P(T<=t) one-tail	1.1573E-23	
	t Critical one-tail	1.67655089	
	P(T<=t) two-tail	2.3145E-23	
	t Critical two-tail	2.00957524	
Boquillas	t-Test: Two-Sample Assuming Unequal Variances		
		Variable 1	*Variable 2*
	Mean	2.62841009	-8.0960117
	Variance	6.2396515	4.27767391
	Observations	19	19
	Hypothesized Mean Difference	0	
	df	35	
	t Stat	14.4144486	
	P(T<=t) one-tail	1.3731E-16	
	t Critical one-tail	1.68957246	
	P(T<=t) two-tail	2.7462E-16	
	t Critical two-tail	2.03010793	

Figure 9 T-tests for each field site location ($\delta^{18}O_{mod}$) against each site stream water flow (m^3/s^2), respectively. Using the average $\delta^{18}O_{wv}$. All significantly different.

References

Baillie, Matthew N., James F. Hogan, Brenda Ekwurzel, Arun K. Wahi, and Christopher J. Eastoe. "Quantifying water sources to a semiarid riparian ecosystem, San Pedro River, Arizona." *Journal of Geophysical Research: Biogeosciences,* vol.112, No. 3, 2007.

Barbour, M.M., and Farquhar, G.D. "Relative humidity- and ABA-induced variation in carbon and oxygen isotope ratios of cotton leaves." *Plant, Cell, and* Environment, vol. 23, 2000, pp. 473-485.

Barbour, Margaret M., Roden, John S., Farquhar, Graham D., and Ehleringer, James R. "Expressing leaf water and cellulose oxygen isotope ratios as enrichment above source water reveals evidence of a Peclet Effect." *Springer in cooperation with International Association for Ecology: Oecologia*, vol.138, No. 3, 2004, pp. 426-435.

Brookshire, David S., Goodrich, David, Dixon, Mark D., Brand, L. A., Benedict, Karl, Lanset, Kevin, Thacher, Jennifer, Broadbent, Craig D., Stewart, Steve, McIntosh, Molly, and Kang, Doosun. "Ecosystem Services and Reallocation Choices: A Framework for Preserving Semi-Arid Regions in the Southwest." *Journal of Contemporary Water Research & Education*, vol. 144, No. 1, Mar. 2010, pp. 60–74.

Bowen, Gabriel. "Global and Regional Maps of Isotope Ratios in Precipitation." WaterIsotopes.org, 2019, wateriso.utah.edu/waterisotopes/pages/data_access/figures.html.

Busch D, Ingraham N, Smith S. "Water uptake in woody riparian phreatophytes of the southwestern United States: a stable isotope study." *Ecological Applications,* vol. 2, No. 4, 1992, pp. 450–459.

Celle-Jeanton H, Travi Y, Blavoux B. "*Isotopic typology of the precipitation in the Western Mediterranean Region at three different time scales.*" *Geophysical Research Letters,* vol. 28 No. 7, 2001, pp. 1215–1218.

Cernusak, L.A., Wong, S-C., Farquhar, G.D. "Oxygen isotope composition of phloem sap in relation to leaf water in Ricinus communis." *Funct Plant Biol*, vol. 30, 2003, pp. 1059–1070.

Delattre H, Vallet-Coulomb C, Sonzogni C. "Deuterium excess in atmospheric water vapor of a Mediterranean coastal wetland: regional versus local signatures." *Atmospheric Chemistry and Physics Discussions*, vol. 15, No. 2, 2015, pp. 1703–1746.

Farid, A., Goodrich, D.C., Bryant, R., and Sorooshian, S. “Using airborne lidar to predict Leaf Area Index in cottonwood trees and refine riparian water-use estimates.” *Journal of Arid Environments,* vol. 72, 2008, pp. 1-15.

Farquhar G.D., Lloyd J. “Carbon and oxygen isotope effects in the exchange of carbon dioxide between terrestrial plants and the atmosphere.” *Stable Isotopes and Plant Carbon-Water Relations*, 1993, pp 47–70.

Farquhar GD, Hubick KT, Condon AG, Richards RA. “Carbon isotope discrimination and water-use efficiency.” *Stable Isotopes in Ecological Research,* 1989, pp 21–46.

Gazal, Rico M., Scott, Russell L., Goodrich, David C., and Williams, David G. “Controls on transpiration in a semiarid riparian cottonwood forest.” *Agricultural and Forest Meteorology,* vol. 137, 2006, pp. 56-67.

Helliker, B. R. and Ehleringer, J.R. «Differential 18O enrichment of leaf cellulose in C3 *versus* C4 grasses.” *Funct. Plant Biol,* vol. 29, 2002, pp. 435-442.

Hickman, et al. “Pest Notes: Wood Decay Fungi in Landscape Trees.” UC IPM, UC ANR , ipm.ucanr.edu/PMG/PESTNOTES/pn74109.html.

Kochendorfer, John, Castillo, Eugenia G., Haas, Edward, Oechel, Walter C., and Paw U, Kyaw Tha. “Net ecosystem exchange, evapotranspiration, and canopy conductance in a riparian forest.” *Agriculture and Forest Meteorology,* vol. 151, Dec. 2010, pp. 544-553.

Leffler, A. J. and Evans, and Ann S. “Variation in carbon isotope composition among years in the riparian tree *Populus fremontii*.” *Oecologia,* vol. 119, Feb. 1999, pp. 311-319.

Magnani, F., Leonardi, S., Tognetti, R., Grace, J., Borghetti, M. “*Modelling the surface conductance of a broadleaf canopy: effects of partial decoupling from the atmosphere*. *Plant, Cell Environment,* vol. 21, 1998, pp. 867–879.

Majoube, M. "Fractionnement en oxygene-18 et en deuterium entre l’eau et sa vapeur." *Chem Phys*, vol. 58, 1971, 1423-1436.

Meixner, Thomas, Leavitt, Steven W., and Morina, Kiyomi. "Water Sources over time for a semi arid river – Implications for water resources." *University of Arizona, Department of Hydrology and Atmospheric Sciences and Laboratory of Tree Ring Research,* 2016.

Merlivat, L. “Molecular diffusivities of $H_2{}^{16}O$, $HD_2{}^{16}O$, and $H_2{}^{18}O$ in gases. *J Chem Phys,* vol. 69, 1978, pp. 2864-2871.

Microsoft Excel. Microsoft Corporation, Microsoft Office 365 ProPlus, Analysis ToolPak Add-In, version 2016.

Nichols, M. H., and E. Anson. “Southwest Watershed Research Center Data Access Project." *Water Resources Research*, vol. 44, 2008, W05S03, doi:10.1029/2006WR005665. http://dx.doi.org/10.1029/2006WR005665 http://pubag.nal.usda.gov/catalog/17974

Pataki, D. E., Bush, S. E., Gardner, P., Solomon, D. K., and Ehleringer, J. R. “Ecohydrology in a Colorado river riparian forest: implications for the decline of *Populus fremontii*.” *Ecological Applications*, vol. 15, 2005, pp. 1009-1018.

Roden, J.S., and Ehleringer, J.R. “Hydrogen and oxygen isotope ratios of tree-ring cellulose for riparian trees grown long-term under hydroponically controlled environmnets.” *Oecologia*, vol 121, August 1999, pp. 467-477.

Roden, J. S., Lin, G., Ehleringer, J.R. “A mechanistic model for interpretation of hydrogen and oxygen isotope ratios in tree-ring cellulose.” *Geochimica et Cosmschimica Acta*, vol 64, No. 1, May 1999, pp. 21-35.

Sargeant, Christopher I. and Singer, Michael B. “Sub-annual variability in historical water source use by Mediterranean riparian trees.” *Ecohydrology,* vol. 9, Mar. 2016, pp. 1328-1345.

Schaeffer, Sean M., Williams, David G., and Goodrich, David C. “Transpiration on cottonwood/willow forest estimated from sap flux.” *Agriculture and Forest Meteorology,* vol. 105, 2000, pp. 257-270.

Singer, MB, Sargeant, CI, Evans, C, “A tool for back-calculating isotopic signatures of water sources used by vegetation,” 2018, doi:10.5281/zenodo/1161221

Snyder, Keirith A., and David G. Williams. "Water sources used by riparian trees varies among stream types on the San Pedro River, Arizona." *Agricultural and Forest Meteorology*, vol. 105, no. 1, 2000, pp. 227-240.

Song, X., Barbour, M.M., Farquhar, G.D., Vann, D.R., and Helliker, B.R. “Transpiration rate relates to within- and across-species variations in effective path length in a leaf water model of oxygen isotope enrichment.” *Plant, Cell and Environment,* vol. 36, 2013, pp. 1338-1351

Southwest Watershed Research Center. “The Southwest Watershed Research Center Data Access Project (DAP).” *USDA Agricultural Research Service*, 2017 https://data.nal.usda.gov/dataset/southwest-watershed-research-center-data-access-project-dap

Sterberg and DeNiro.”Biogeochemical implications of the isotopic equilibrium fractionation factor between oxygen atoms of acetone and water.” *Geochim Cosmochim Acta,* vol. 47, 1983, pp. 2271-2274.

Vitousek, P. M. “Biological invasions and ecosystem processes: towards an integration of population biology and ecosystem studies.” *Oikos*, vol. 57, 1990, pp. 7-13.